

DOKOUPIL

ON THE EQUILIBRIUM BETWEEN THE  
SOLID AND THE GAS PHASE OF THE  
SYSTEMS HYDROGEN-NITROGEN,  
HYDROGEN - CARBON MONOXIDE  
AND HYDROGEN-NITROGEN-  
CARBON MONOXIDE

Z. DOKOUPIL

Universiteit Leiden

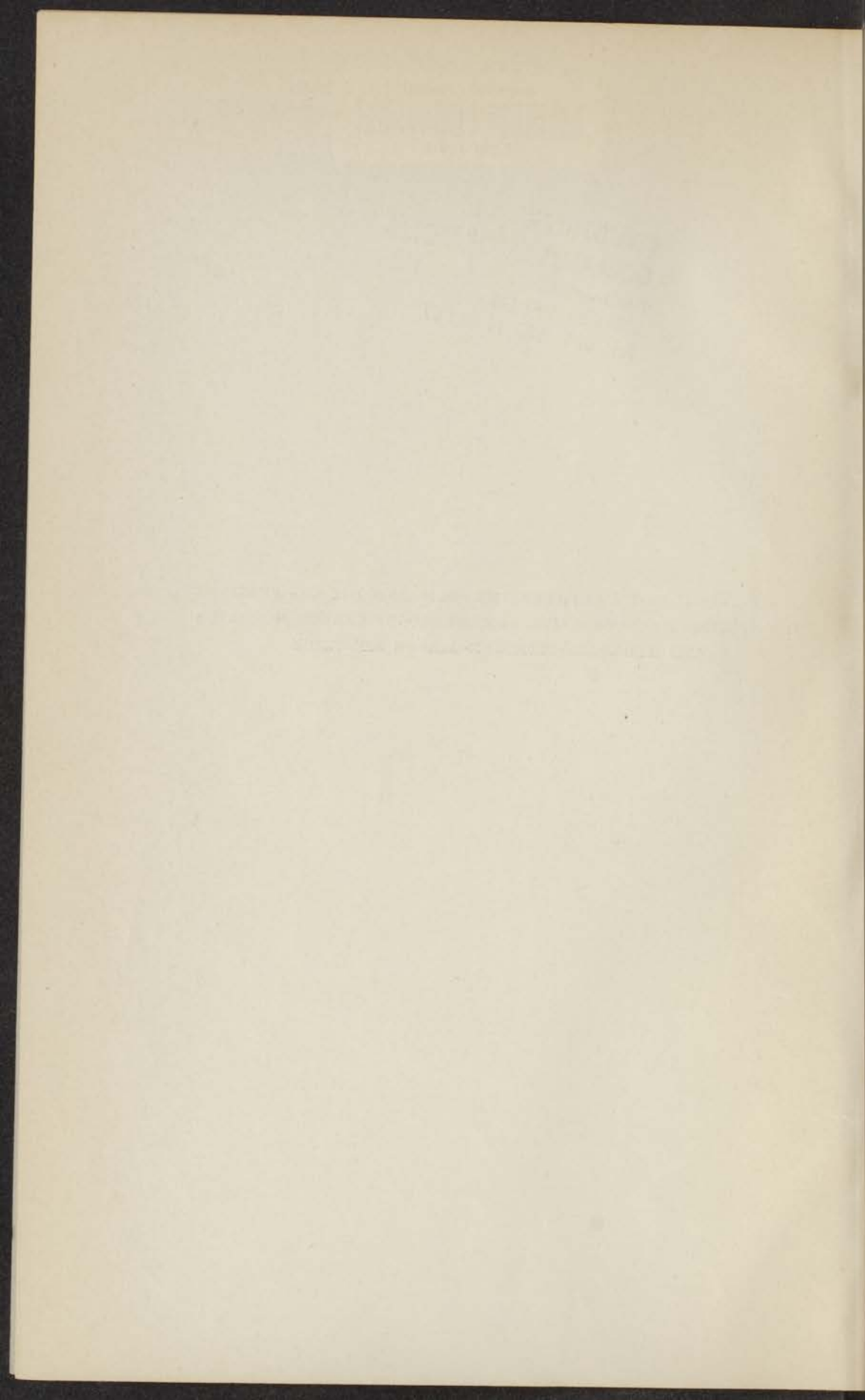


1 481 139 7

Hoogleeraar  
Dr. J. J. HERMANS

BIBLIOTHEEK  
GORLAEUS LABORATORIA  
Postbus 9502  
2300 RA LEIDEN  
Tel.: 071 - 527 43 66 / 67

ON THE EQUILIBRIUM BETWEEN THE SOLID AND THE GAS PHASE OF  
THE SYSTEMS HYDROGEN-NITROGEN, HYDROGEN-CARBON MONOXIDE  
AND HYDROGEN-NITROGEN-CARBON MONOXIDE



ON THE EQUILIBRIUM BETWEEN THE  
SOLID AND THE GAS PHASE OF THE  
SYSTEMS HYDROGEN-NITROGEN,  
HYDROGEN-CARBON MONOXIDE  
AND HYDROGEN-NITROGEN-  
CARBON MONOXIDE

PROEFSCHRIFT

TER VERKRIJGING VAN DE GRAAD VAN DOCTOR IN DE  
WIS- EN NATUURKUNDE AAN DE RIJKSUNIVERSITEIT  
TE LEIDEN OP GEZAG VAN DE RECTOR-MAGNIFICUS  
DR J. N. BAKHUIZEN VAN DEN BRINK,  
HOGLERAAR IN DE FACULTEIT DER GODGELEERDHEID,  
TEGEN DE BEDENKINGEN VAN DE FACULTEIT  
DER WIS- EN NATUURKUNDE TE VERDEDIGEN  
OP WOENSDAG 6 APRIL 1955 TE 16 UUR

DOOR

ZDENĚK DOKOUPIL

GEBOREN TE SVIADNOV (TSJECHOSLOWAKIJE)  
IN 1920



'S-GRAVENHAGE  
MARTINUS NIJHOFF  
1955

ON THE CATALYTIC ACTIVITY OF  
THE CHLORIDE OF THE  
HYDROGEN-NITROGEN  
AND CARBON MONOXIDE  
AND HYDROGEN-NITROGEN  
AND CARBON MONOXIDE

THESIS

BY  
DR. K. W. TACONIS

*Promotor:* Prof. Dr K. W. TACONIS

AMSTERDAM

1955

RESEARCH REPORT

NO. 10

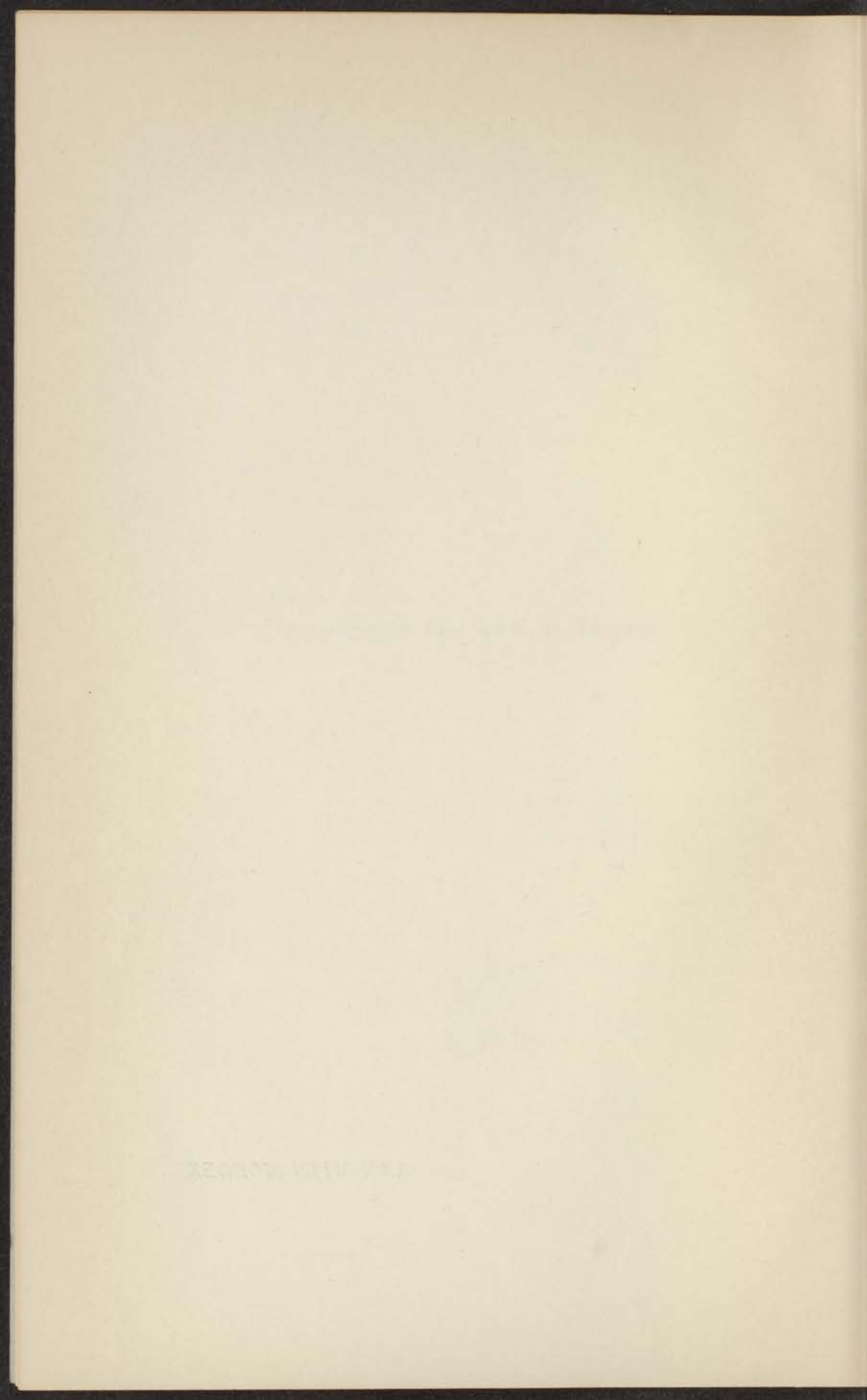


AMSTERDAM

MAKINGE WILHELM

1955





## CONTENTS

<i>Introduction</i> . . . . .	1
Chapter I. Phase equilibrium of a binary system . . . . .	3
§ 1. Phase equilibrium and equilibrium diagrams . . . . .	3
§ 2. Behaviour of the binary system nitrogen-carbon monoxide. . . . .	5
§ 3. Behaviour of the binary system hydrogen-nitrogen	8
Chapter II. Theoretical determination of equilibrium curves .	12
§ 4. Effect of an inert gas on a univariant equilibrium .	12
§ 5. Beattie-Bridgeman equation of state . . . . .	15
§ 6. Integration of the equilibrium formula . . . . .	17
§ 7. Calculation of the coefficients for the $H_2-N_2$ mixture in the equation of state . . . . .	18
§ 8. Numerical evaluation of the linear theory . . . . .	23
Chapter III. Experimental determination of the equilibrium curves . . . . .	27
§ 9. Experimental methods for the determination of the equilibrium curves . . . . .	27
§ 10. Cryostat and equilibrium vessel for the flow method	29
§ 11. Apparatus for analysis of a binary gas mixture . .	31
Chapter IV. Experimental results of the system hydrogen- nitrogen and hydrogen-carbon monoxide . . . . .	34
§ 12. Experimental data of the mixture hydrogen-nitrogen	34
§ 13. Experimental data of the mixture hydrogen-carbon monoxide . . . . .	35

§ 14. Sources of error . . . . .	40
§ 15. Discussion of results . . . . .	41
Chapter V. Comparison of theory and experiment . . . . .	45
§ 16. General $p,T$ -theory . . . . .	45
§ 17. General $V,T$ -theory . . . . .	49
Chapter VI. The ternary system hydrogen-nitrogen-carbon monoxide . . . . .	51
§ 18. Two-phase equilibrium of a three component system	51
§ 19. Experimental method for investigation of the ternary system hydrogen-nitrogen-carbon monoxide	52
§ 20. Experimental data of the mixture hydrogen-nitro- gen-carbon monoxide . . . . .	54
<i>References</i> . . . . .	59
<i>Samenvatting</i> . . . . .	60

### Summary

The equilibrium between the solid and gas phases has been studied, using the flow method. The pressure varied from 1.3 atm up to 50 atm. The composition of the gas phase has been determined by means of the solidification of  $N_2$  (or CO) with the aid of liquid hydrogen. The most favourable conditions for the purification of hydrogen were deduced from the experimental results with respect to the binary mixtures  $H_2-N_2$  and  $H_2-CO$ . The agreement between theory and experiments proved to be satisfactory. The behaviour of the ternary mixture  $H_2-N_2-CO$  is shown in the corresponding diagrams.

*Introduction.* Hydrogen is one of the most important elements in nature. Soon after its discovery hydrogen was isolated and its properties were studied. The use of hydrogen in low temperature laboratories, as a raw material for the synthesis of ammonia in chemical industries and recently in the separation of deuterium gives a few examples of its most important applications. The preparation of pure hydrogen still plays an important rôle in science and industry.

The method of production of pure hydrogen is, of course, governed by the cost of production, especially if there is a need for large quantities of hydrogen. In general we may say that the use of the purest possible hydrogen is necessary in continuous processes, because a negligibly small quantity of impurities present may lead to serious difficulties by their cumulative effect. For instance, slightly contaminated hydrogen can block the heat exchangers

during its liquefaction, while in the case of synthesis of ammonia, where a large quantity of hydrogen is required, the efficiency of the catalysts in this process can be seriously decreased.

On a large scale, hydrogen can be produced by the separation of coke-oven gas by means of low temperature methods. The typical composition of the latter is about 50%  $H_2$  + 28%  $CH_4$  + 10%  $N_2$  + 7%  $CO$  + 3%  $C_nH_m$  + 2%  $CO_2$ . The removal of higher hydrocarbons, carbon dioxide and methane is relatively easier than that of nitrogen and carbon monoxide; this is due to the lower critical temperatures of both the latter components. As a result of this method of hydrogen production we can always expect the presence of small quantities of impurities which consist mainly of nitrogen and carbon monoxide.

The separation of gases at low temperatures is, of course, based on the laws of thermodynamics. It would be of no use to start the separation procedure in the gaseous phase with all the components of the system hydrogen-nitrogen-carbon monoxide because all gases are completely miscible. But if we have several phases of the above mentioned system, the equilibrium between the different phases will be established at the same temperature and pressure; moreover, the chemical potential of each component will be the same in every phase. On the other hand, with some exceptions the concentration in the various phases will differ: this property constitutes the basis of the separation methods. The general Gibbs equilibrium condition is the starting point for the theoretical calculations which may predict quite well the actual behaviour of the observed system, or on the other hand the theory may help us to understand the experimental results. The combination of theory and experiment is, therefore, of the utmost importance in interpreting equilibrium problems.

The characteristic behaviour of a system consisting of two or more components in several phases can be represented quantitatively by phase diagrams. The above mentioned system, hydrogen-nitrogen-carbon monoxide, and all binary systems of its respective components have been measured principally in the case of equilibrium between the gas and liquid phases by various authors. We know from their experiments that there is an appreciable concentration of nitrogen or carbon monoxide down to about 63°K, the triple-point temperature of nitrogen. Therefore, the question arises: what happens with the nitrogen and carbon monoxide at lower

temperatures at various pressures? This, in other words, implies the study of the equilibrium between the gaseous and the solid phase of the hydrogen systems.

The present work deals with the theoretical and experimental investigation of the equilibria of the hydrogen systems below the triple-point temperature of nitrogen down to the critical temperature of hydrogen; the pressure range covers the region from 50 atm down to 1.3 atm.

The first chapter gives a qualitative survey of the binary systems nitrogen-carbon monoxide and hydrogen-nitrogen, in the whole temperature and pressure range; we have indicated the field of our interest in the corresponding diagrams. The theoretical approach is developed in chapter II by the application of the general equation of state of a binary gas mixture to the two-phase equilibrium between the gas and the solid states. The general experimental procedure is explained in chapter III which also contains the description of the analytical equipment, especially designed for the determination of very low concentrations of nitrogen or carbon monoxide in hydrogen. The results of both binary systems, hydrogen-nitrogen and hydrogen-carbon monoxide, are collected and discussed in the following chapter IV. The theoretical predictions are compared with the measurements in the subsequent chapter V.

The investigations of the above-mentioned binary systems already gave a sufficient basis to design roughly the ternary equilibrium diagrams. But it seemed desirable to us to have the specific knowledge of the position of the connodal lines which determine the relative concentration shift of both condensable components with respect to the initial concentration of carbon monoxide and nitrogen. After making a slight change of the analytical apparatus we determined directly the gas curves of the complete ternary system in some typical cases. These results are included in the last chapter VI.

## CHAPTER I. PHASE EQUILIBRIUM OF A BINARY SYSTEM

§ 1. *Phase equilibrium and equilibrium diagrams.* The state of a homogeneous system consisting of one component X forms the most simple thermodynamic system in one phase. There are two degrees of freedom: for instance, the temperature  $T$  and the pressure  $p$ . Two different phases 1 and 2 will be characterized by two pairs of values

$p_1, T_1$  and  $p_2, T_2$ . In the equilibrium of both phases the number of degrees of freedom is reduced to one; moreover, equilibrium can subsist only if the temperature and the pressure are the same in both phases; therefore, if the pressure is fixed, only one temperature corresponds to a state of equilibrium. The maximum number of phases in equilibrium is three with no degree of freedom at all.

The familiar representation of a system of only one component is given by the  $p, T$ -diagram covering the whole range of pressures and temperatures: any state of a system in one phase is represented by one point with the coordinates  $p, T$ ; all such points fill up a homogeneous region bordered at some places by curves which correspond to the two-phase equilibrium; for instance, the vapour pressure curves of the liquid or of the solid state of the pure component X. In this representation the three-phase equilibrium is located by points known as triple-points.

When we consider a homogeneous system of two components X and Y, we refer the concentration of both components to their mole fractions  $x$  and  $y$  which are, of course, connected by the relation  $x + y = 1$ . The binary system in one phase has three degrees of freedom, for instance  $p, T$ , and  $x$ . Two different phases 1 and 2 will be characterized by two triplets of values  $p_1, T_1, x_1$  and  $p_2, T_2, x_2$ . At the equilibrium of both phases, the pressure and the temperature will be the same and the number of degrees of freedom will be two; for instance, at fixed  $p$  ( $= p_1 = p_2$ ) and  $T$  ( $= T_1 = T_2$ ), the two concentrations will establish themselves. At the equilibrium of three phases there is one degree of freedom, for instance  $p$ : indeed the choice of the pressure determines  $T, x_1, x_2$  and  $x_3$  for the three coexisting phases. The maximum number of phases in the equilibrium of a binary mixture is four: as there is no degree of freedom left, this case may be realized only at a certain pressure  $p$ , a temperature  $T$  and the concentrations  $x_1, x_2, x_3$  and  $x_4$  in the four phases respectively.

The complete binary system can be represented in the whole pressure and temperature interval by means of a three-dimensional space figure <sup>1)</sup> which is referred to the three coordinate axes  $p, T$  and  $x$ . Thus the homogeneous state in any phase is given by a point. The two-phase equilibrium is represented by two points  $p, T, x_1$  and  $p, T, x_2$ ; a line joining these two points and perpendicular to the  $p, T$ -plane is called the connodal or tie-line. All possible pairs of these points give rise to two equilibrium surfaces, for instance, the gas and

the liquid surfaces. The space between the two equilibrium surfaces is known as the inhomogeneous region. The three-phase equilibria are given by the triplets of points  $p, T, x_1$ ,  $p, T, x_2$  and  $p, T, x_3$ ; the middle point trajectory is called the three-phase line. In this case the connodal lines fill up a cylindrical surface perpendicular to the  $p, T$ -plane with the three-phase line as a directrix. The four-phase equilibrium is to be found on the connodal line with four points  $p, T, x_1$ ,  $p, T, x_2$ ,  $p, T, x_3$ , and  $p, T, x_4$  thereupon; this state is known as a quadruple-point with respect to the  $p, T$ -plane.

Instead of constructing the three-dimensional space figure we can determine a set of two-dimensional equilibrium diagrams having one of the three parameters  $p, T$ , or  $x$  constant. Keeping  $x$  constant gives rise to a system of figures analogous to the  $p, T$ -diagram of both pure components for  $x = 0$  or  $x = 1$  respectively. More frequently we take fixed values of the pressure  $p$  (or the temperature  $T$ ) and plot the temperature (or the pressure  $p$ ) as a function of the concentration  $x$  between the values 0 and 1.

For the ternary system of three components X, Y, and Z (the concentrations are  $x, y$ , and  $z$  respectively, connected by  $x + y + z = 1$ ) a four-dimensional model would be of some advantage. One phase is given by four coordinates  $p, T, x, y$ ; a two-phase equilibrium gives rise to three-dimensional hypersurfaces; the three-phase equilibria are determined by the three-phase surfaces; the four-phase equilibria are characterized by the quadruple-lines and the five-phase equilibria are restricted to the quintuple-points.

It would be possible to hold one parameter constant, for instance the pressure  $p$ , and to consider the set of resulting three dimensional figures. For practical purposes, however, one keeps two parameters constant (in the case of interest to us, for example, the pressure  $p$  and the temperature  $T$ ) and the whole ternary system can, thus, be represented by a double set of familiar triangular diagrams which give the concentrations of phases in equilibrium for every pair of values  $p, T$  separately.

§ 2. *Behaviour of the binary system nitrogen-carbon monoxide.* On the basis of the representation methods explained in the previous section we shall first discuss the system nitrogen-carbon monoxide. Both constituent components  $N_2$  and CO show a great physical and chemical similarity and the system of such components will, there-

fore, principally differ from a system, of which the critical points of the two components are far apart, as for instance in the system hydrogen-nitrogen. Here we shall neglect the presence of the transition between the modifications  $\alpha$  and  $\beta$  in the solid phase of  $N_2$  or CO.

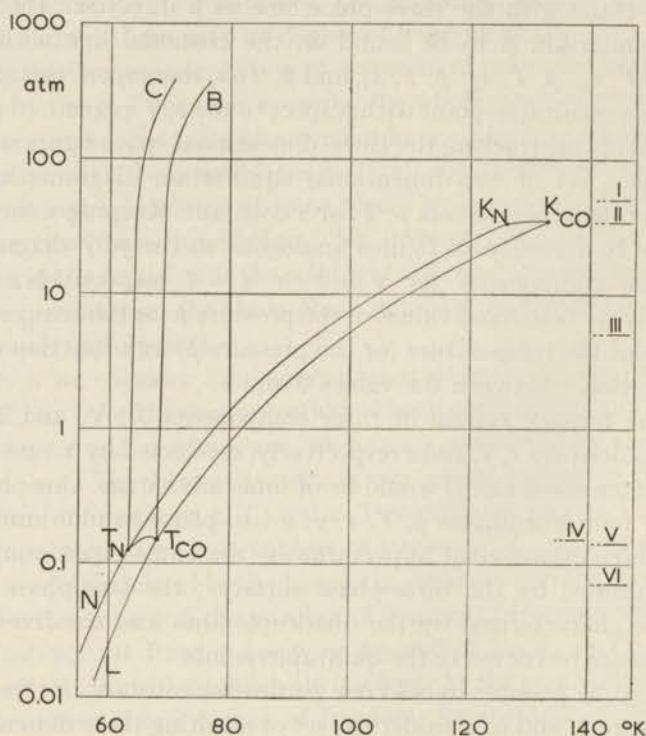


Fig. 1.  $p, T$ -diagram of CO- $N_2$ -mixture.

Fig. 1 gives the  $p, T$ -diagram of the  $N_2$ -CO mixture; because of the large pressure interval we plotted the pressure logarithmically along the vertical axis and the temperature linearly along the horizontal axis. The properties of pure nitrogen are given by the triple-point  $T_N$ , the vapour pressure curve  $T_N$ - $K_N$ , the melting curve  $T_N$ -C and the sublimation curve  $T_N$ -N. Carbon monoxide is similarly characterized by its triple-point  $T_{CO}$ , the critical point  $K_{CO}$  the vapour pressure curve  $T_{CO}$ - $K_{CO}$ , the melting curve  $T_{CO}$ -B and the sublimation curve  $T_{CO}$ -L. The curve  $T_N$ - $T_{CO}$  represents the unique three-phase line of the system. We used the data given by Ver-

schoyle<sup>2)</sup> and National Bureau of Standards<sup>3)</sup> for the plotting of these curves. The actual position of the critical line  $K_N-K_{CO}$  will not appreciably differ from the proposed curve.

With the help of the  $p, T$ -diagram we can with advantage choose a set of characteristic  $T, x$ -diagrams shown in fig. 2, for six different pressures  $p_I, p_{II}, \dots, p_{VI}$ . The subscripts I, II,  $\dots$ , VI correspond to the series of  $T, x$ -sections of the space figure. The temperature  $T$  and the concentration  $x$  are plotted linearly, G represents a gas phase, L the liquid phase and S the solid phase; a sum of two of these symbols signifies the inhomogeneous region corresponding to the same phases. The horizontal connodals are drawn only for the case of a three-phase equilibrium.

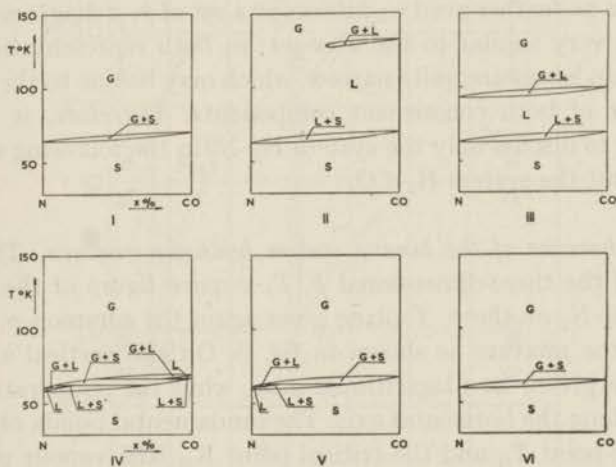


Fig. 2.  $T, x$ -isobars of  $CO-N_2$ -mixture.

At the pressure  $p_I$  above the critical line of the system only the equilibrium between the gas and the solid phase will be established as shown in diagram I, in accordance with the complete solubility of both components in the condensed states. If the pressure is decreased to the value  $p_{II}$  between the critical pressure of  $CO$  and  $N_2$  the inhomogeneous region  $G + L$  will commence to spread out, as shown in diagram II, and will soon reach the  $N_2$ -axis. If we further decrease the pressure, the  $G + L$  region will move downwards toward the  $L + S$ -lens with respect to the different slopes of the vapour pressure curve and the melting curve; this is represented in diagram III. Both regions  $G + L$  and  $L + S$  make a point of contact

at the pressure equal to the maximum of the three-phase line; this will be the first three-phase equilibrium. When the pressure has the value  $p_{IV}$  lower than the above mentioned maximum of the three-phase line, but still higher than both triple-points, the new inhomogeneous region will be established as shown in diagram IV. By reducing the pressure to the value  $p_V$  below the triple-point of CO this new region G + S will reach the CO-axis as shown in diagram V. Finally, at pressures below the triple-point of nitrogen the region G + L totally vanishes, and only the region G + S remains so that the last diagram looks like the first one from which we started. This remaining equilibrium lens G + S, however, will shift downwards along the sublimation lines faster than before.

There is no further need to determine a set of  $p, x$ -diagrams which would be very similar to the  $T, x$ -set; in both representations the equilibrium lenses are quite narrow, which may be due to the similar behaviour of both constituent components. Therefore, it will be sufficient to discuss only the system  $H_2-N_2$  in the following section, and to omit the system  $H_2-CO$ .

§ 3. *Behaviour of the binary system hydrogen-nitrogen.* The projection of the three-dimensional  $p, T, x$ -space figure of the binary system  $H_2-N_2$  on the  $p, T$ -plane gives again the common  $p, T$ -diagram of the mixture as shown in fig. 3. On the vertical axis the pressure is given, on a logarithmic scale, while the temperature can be read along the horizontal axis. The fundamental points of  $H_2$  are the triple-point  $T_H$  and the critical point  $K_H$ ; the vapour pressure curve  $T_H-K_H$ , the melting curve  $T_H-D$  and the sublimation curve  $T_H-M$  subsequently determine the properties of pure hydrogen <sup>4</sup>). The corresponding points and curves for nitrogen are the triple-point  $T_N$ , the critical point  $K_N$ , the vapour pressure curve  $T_N-K_N$ , the melting curve  $T_N-C$  and the sublimation curve  $T_N-N$ .

For the behaviour of the binary mixture of  $H_2-N_2$  the critical line and the three-phase lines are of importance. The critical line  $K_H-K_N$  is connecting both critical points which are in this case far apart. Further it will be assumed that there is no complete solubility of both components in the solid state; we shall again neglect the  $\alpha \rightarrow \beta$ -transition of nitrogen at about 35°K. For the sake of brevity we shall use in this section the symbol G for a gas phase, L for the liquid phase, S for the solid nitrogen and S' for solid hydrogen. The first

three-phase line  $T_N-Q$  determines the equilibrium  $S + L + G$ ; actually this line is divided by the critical line into two separate parts  $T_N-A$  and  $B-Q$ . The second three-phase line  $T_H-Q$  gives rise to the equilibrium  $L + G + S'$ . The third three-phase line  $E-Q$  leads to the equilibrium  $S + L$  (or  $G$ )  $+ S'$ . The last three-phase line  $F-Q$  characterizes the equilibrium  $S + G + S'$ . In this  $p, T$ -representation all three-phase lines intersect each other in the quadruple-point  $Q$  where the four-phase equilibrium  $S+L+G+S'$  will be established.

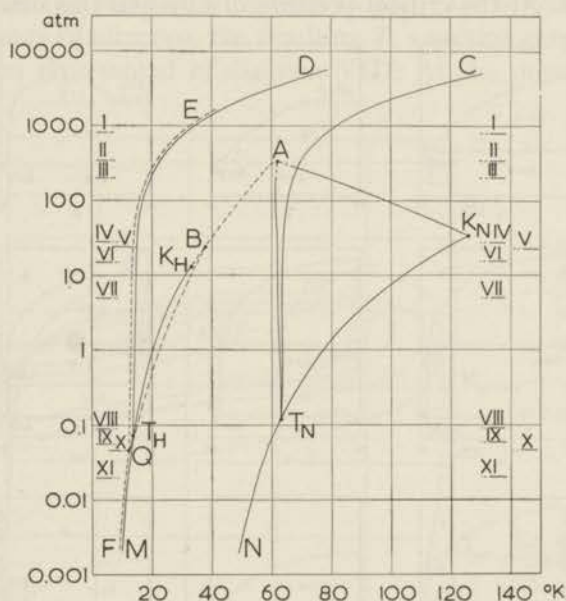


Fig. 3.  $p, T$ -diagram of  $H_2-N_2$ -mixture.

The full curves are drawn according to the known experimental data. We added to the diagram the dotted lines which we suppose to be the most probable curves on the basis of the study of the behaviour of other appropriate binary mixtures at high temperatures.

The construction of a set of some typical sections through the space figure will provide us with more information about the properties of the binary system than the  $p, T$ -diagram only. The  $T, x$ -sections in fig. 4 are denoted by the same symbols I, II, ... XI which correspond to the pressures  $p_I, p_{II}, \dots, p_{XI}$  in fig. 3. The temperature  $T$  is plotted linearly in the diagrams; on the other hand,

it was necessary to enlarge appreciably the concentration scale in the neighbourhood of the hydrogen axis; this deformation, however, does not affect the qualitative discussions of the system  $H_2-N_2$ .

If the pressure is above the maximum of the critical line, the resulting diagram I will be similar to the known case of a solid-liquid equilibrium. Supposing the pressure  $p_{II}$  to be at the point A on the critical line, the three-phase connodal line appears in the diagram II. On decreasing the pressure to the value  $p_{III}$  the inhomogeneous region  $L + G$  takes the form given by *Verschöyle*<sup>2)</sup> in the diagram III. At the critical pressure of nitrogen this new inhomogeneous region  $L + G$  will reach the  $N_2$ -axis; the point of contact, of course, will coincide with the critical temperature of nitrogen. The

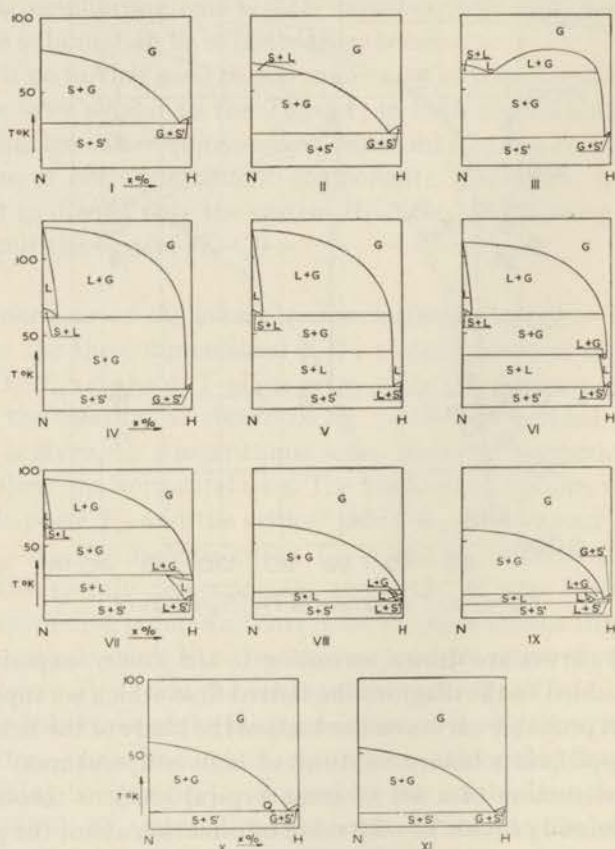


Fig. 4.  $T, x$ -isobars of  $H_2-N_2$ -mixture.

geneous region  $L + G$  will reach the  $N_2$ -axis; the point of contact, of course, will coincide with the critical temperature of nitrogen. The

L + G-part of the equilibrium diagram will move downwards with decreasing pressure as shown in diagram IV. The pressure  $p_V$  corresponding to the second intersection point B of the critical line with the three-phase line  $T_N-Q$ , gives rise to a second three-phase temperature shown in diagram V; on decreasing further the pressure to the value  $p_{VI}$  the new inhomogeneous region L + G spreads out as shown in diagram VI, and will subsequently reach the hydrogen axis at the critical temperature of hydrogen. The typical diagram VII is drawn for a pressure  $p_{VII}$  just below the critical pressure of hydrogen. If the pressure is reduced to  $p_{VIII}$ , i.e. below the triple-point pressure of nitrogen, the resulting  $T, x$ -section gets simplified to the form represented in diagram VIII. At the pressure of the

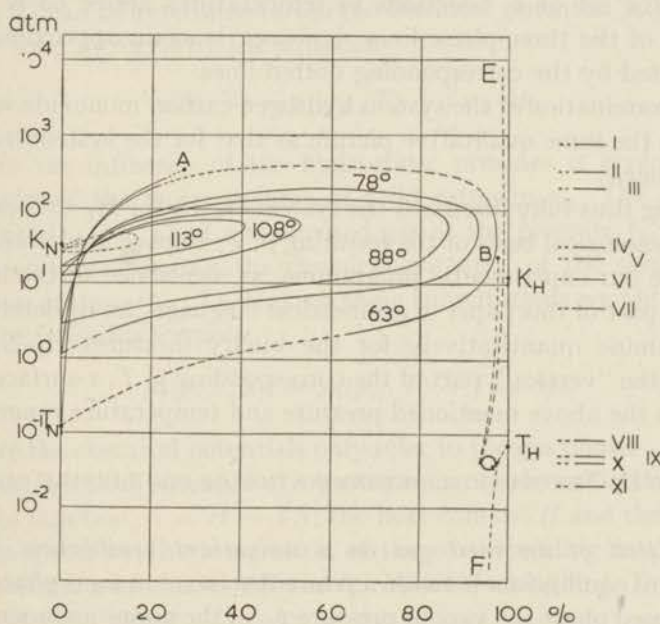


Fig. 5.  $p, x$ -isotherms of  $H_2-N_2$ -mixture.

triple-point of hydrogen both inhomogeneous regions L + G and L + S' come to a contact just on the hydrogen axis, and if the pressure is fixed to the value  $p_{IX}$ , the new three-phase equilibrium L + G + S' will isolate the triangle formed by the homogeneous region L from the hydrogen axis. The four-phase equilibrium S + L + G + S' would be established at the pressure  $p_X$  according

to diagram X, in which the previous liquid region L has been reduced to the point Q. For any pressure  $p_{XI}$  below the quadruple-point pressure the corresponding diagram XI would look just like the first one from which we started.

Instead of the complete set of separate  $p, x$ -sections of the space figure we presented a view of this  $p, T, x$ -space model in fig. 5. The logarithmic scale corresponds to the vertical scale of fig. 3, and the same restriction of the linearity as in fig. 4 applies to the concentration scale of fig. 5. In this representation the curves correspond to the respective  $p, x$ -sections at a constant temperature  $T^\circ\text{K}$  <sup>5)6)</sup>. The profile of the space figure for various constant pressures has already been shown in fig. 4. For the sake of legibility of fig. 5 we limited the set of  $p, x$ -sections to temperatures above  $63^\circ\text{K}$ ; the position of the three-phase lines, however, is again approximately represented by the corresponding dotted lines.

The examination of the system hydrogen-carbon monoxide would result in the same qualitative picture as that for the system hydrogen-nitrogen.

Having thus fully discussed the system  $\text{H}_2\text{-N}_2$  (or  $\text{H}_2\text{-CO}$ ) on the phenomenological basis of the resulting  $p, T, x$ -space model we now can state our experimental programme, as mentioned in the introductory part of this paper in geometrical language: let us determine and examine quantitatively for the binary mixtures  $\text{H}_2\text{-N}_2$  (or  $\text{H}_2\text{-CO}$ ) the "vertical" part of the corresponding  $p, T, x$ -surface (see fig. 5) in the above mentioned pressure and temperature ranges.

## CHAPTER II. THEORETICAL DETERMINATION OF EQUILIBRIUM CURVES

§ 4. *Effect of an inert gas on a univariant equilibrium.* In a univariant equilibrium between a pure substance 1 in a gas phase and a condensed phase the vapour pressure  $p_{01}$  of the pure component is a function of temperature alone. Now let this univariant system be at equilibrium under its vapour pressure  $p_{01}$  and let an inert gas that does not react chemically with substance 1 and is assumed to be insoluble in the condensed phase, be introduced into the system until the total pressure becomes  $p$ . This will be the case of the binary equilibrium of the system  $\text{H}_2\text{-N}_2$  for temperatures between  $60^\circ\text{K}$  and  $35^\circ\text{K}$ .

The theoretical considerations will be limited to this case; the subscript 1 will refer to nitrogen and 2 will refer to hydrogen. The

composition of nitrogen in the gas phase will be given by the mole fraction  $x_1$ . The same would apply to the system  $H_2$ -CO.

When the equilibrium is established between the pure solid nitrogen and the gas mixture of nitrogen and hydrogen at the fixed pressure  $p$  and the temperature  $T$ , the chemical potential of nitrogen is the same in both phases. Equating the chemical potential of nitrogen in hydrogen gas  $\mu_1(p, T, x_1)$  to that of pure solid nitrogen  $\mu_s(p, T)$  subjected to the hydrostatic pressure  $p$ , gives implicitly the fundamental relation for the concentration of nitrogen in the gas phase  $x_1$ , at the pressure  $p$  and the temperature  $T$

$$\mu_1(p, T, x_1) = \mu_s(p, T). \quad (1)$$

$\mu_s(p, T)$  can be determined from the chemical potential  $\mu_s(p_{01}, T)$  of pure solid nitrogen by the equation

$$\mu_s(p, T) = \mu_s(p_{01}, T) + \int_{p_{01}}^p v_{01} dp, \quad (2)$$

where the influence of the hydrostatic pressure is given by the integral of the molar volume of solid nitrogen  $v_{01}$ . The chemical potential  $\mu_s(p_{01}, T)$  of a condensed gas at the pressure  $p_{01}$  and the temperature  $T$  equals the chemical potential of the same gas in vapour state  $\mu_1(p_{01}, T)$ . Making these substitutions we obtain from (1) the following formula:

$$\mu_1(p, T, x_1) = \mu_1(p_{01}, T) + \int_{p_{01}}^p v_{01} dp, \quad (3)$$

where the chemical potentials only refer to the gas phase.

The chemical potential of a pure gas can be determined from the Gibbs function,  $G = H - TS$ ; the heat content  $H$  and the entropy  $S$  are given by the integration of the corresponding fundamental differential relations for  $dH$  and  $dS$ . When working in  $p, T$ -variables we get for  $n$  moles

$$G(p, T) = \int_0^p \left( V - \frac{nRT}{p} \right) dp + nRT \ln p + n(h^0 - Ts^0); \quad (4)$$

the chemical potential of pure gas results from the relation  $\mu = G/n$ :

$$\mu(p, T) = \int_0^p \left( \frac{V}{n} - \frac{RT}{p} \right) dp + RT \ln p + h^0 - Ts^0; \quad (5)$$

the integration constants are

$$h^0 = h_0^0 + \int_{p_{01}}^p c_p dT, \quad (6)$$

$$s^0 = s_0^0 + \int_{p_{01}}^p \frac{c_p}{T} dT,$$

where the integrals are to be evaluated along a zero pressure line, and  $h_0^0$  and  $s_0^0$  are the molar heat content and the entropy for the gas at the reference temperature  $T^0$ ;  $c_p$  is the molar heat capacity at constant pressure. The volume  $V$  is to be expressed as a function of  $p$  and  $T$  according to the equation of state of a pure gas.

The Gibbs function for a gas mixture, consisting of  $n_1$  moles of the component 1 and  $n_2$  moles of the component 2, is given by

$$G(p, T, x_1) = \int_0^p \left( V - \frac{\sum n_i RT}{p} \right) dp + \sum n_i RT \ln px_i + \sum n_i (h_i^0 - Ts_i^0); \quad (7)$$

the partial chemical potential for the  $i^{\text{th}}$  component in the gas mixture results from  $\mu_i = (\partial G / \partial n_i)_{p, T, n}$ :

$$\mu_i(p, T, x_1) = \int_0^p \left[ \left( \frac{\partial V}{\partial n_i} \right)_{p, T, n} - \frac{RT}{p} \right] dp + RT \ln px_i + h_i^0 - Ts_i^0. \quad (8)$$

The integration constants  $h_i^0$  and  $s_i^0$  are the same as in the corresponding eq. (6) for the pure components;  $V$  stands again for the volume as a function of  $p$ ,  $T$  and  $x_1$  following the equation of state for a gas mixture.

We can now substitute  $\mu_1(p_{01}, T)$  given by (5) and  $\mu_1(p, T, x_1)$  given by (8) in (3) and obtain the resulting equation for the mole fraction  $x_1$  of nitrogen in the gas mixture and the vapour pressure  $p_{01}$  of pure solid nitrogen at the total pressure  $p$  and the temperature  $T$  ?):

$$RT \ln \frac{px_1}{p_{01}} = - \int_0^p \left[ \left( \frac{\partial V}{\partial n_1} \right)_{p, T, n} - \frac{RT}{p} \right] dp + \int_0^{p_{01}} \left( \frac{V}{n} - \frac{RT}{p} \right) dp + \int_{p_{01}}^p v_{01} dp. \quad (9)$$

The first integral refers to the gas mixture, the second to the pure nitrogen and the third to the condensed nitrogen.

Thus starting from the known vapour pressure  $p_{01}$  we can calculate for any total pressure  $p$  and temperature  $T$  the "enhancement factor"  $f$  given by

$$f = px_1/p_{01}. \quad (10)$$

This quantity  $f$  defines the ratio of the partial pressure  $px_1$  of nitrogen in hydrogen and the vapour pressure  $p_{01}$  of pure nitrogen. For an ideal gas law the effect may be obtained by placing the first and the second integral equal to zero. So in general the mole fraction  $x_1$  of a vapour in a gas mixture is greater than that computed by Dalton's law (sometimes to the extent of 100 times or even more).

§ 5. *Beattie-Bridgeman equation of state.* The integration of (9) requires the knowledge of the equation of state for a pure gas and that for a gas mixture. The Beattie-Bridgeman equation of state proved to give satisfactory results in cases similar to our problems.

The complete equation of state for a pure gas is according to Beattie<sup>8)</sup>

$$p = \frac{RT(1 - c/VT^3)}{V^2} [V + B(1 - b/V)] - \frac{A}{V^2} (1 - a/V). \quad (11)$$

It contains five adjustable constants:  $A$ ,  $B$ ,  $c$ ,  $a$ ,  $b$ . The last two constants  $a$ ,  $b$  represent a second order approximation. When (11) is written out in full and the terms are rearranged in powers of  $1/V$ , we get the virial form of the equation of state:

$$p = \frac{RT}{V} + \frac{\beta}{V^2} + \frac{\gamma}{V^3} + \frac{\delta}{V^4}, \quad (12)$$

where

$$\begin{aligned} \beta &= RTB - A - Rc/T^2, \\ \gamma &= -RTBb + Aa - RBc/T^2, \\ \delta &= RBbc/T^2. \end{aligned}$$

For low pressures and densities one gets the ideal gas equation. The function  $\beta(T)/RT$  gives the normal dependence of the second virial coefficient upon the temperature; there is one real root giving the Boyle temperature;  $\beta/RT$  increases from the negative values to the

positive ones and approaches the limiting value  $B$  as is the case for most gases.

For the integration of the equilibrium condition in  $p, T$ -variables, however, it will be convenient to solve explicitly for the volume as a function of the pressure; this may be achieved by an iterative procedure which gives the following result:

$$V = \frac{RT}{p} + \frac{\beta}{RT} + \left(-\frac{\beta^2}{RT} + \gamma\right) \frac{p}{(RT)^2} + \left(\frac{2\beta^3}{(RT)^2} - \frac{3\beta\gamma}{RT} + \delta\right) \frac{p^2}{(RT)^3} + \dots \quad (13)$$

An equation of state of a gas mixture is an equation expressing the pressure of the mixture in terms of the volume, temperature, the mole fractions and the constants of the equation of state of the pure constituent gases. Usually it has the same form as that of a pure component. As has been shown by Beattie and coworkers<sup>7) 9)</sup> the equation of state for  $\Sigma n_i$  moles of a gas mixture will be best represented by the following equation with the corresponding combination rules of the constants:

$$p = \frac{\Sigma n_i RT}{V} + \frac{(\Sigma n_i)^2 \beta_m}{V^2} + \frac{(\Sigma n_i)^3 \gamma_m}{V^3} + \frac{(\Sigma n_i)^4 \delta_m}{V^4} \quad (14)$$

with

$$\begin{aligned} \beta_m &= RTB_m - A_m - Rc_m/T^2, \\ \gamma_m &= -RTB_m b_m + A_m a_m - RB_m c_m/T^2, \\ \delta_m &= RB_m b_m c_m/T^2, \end{aligned}$$

and

$$\begin{aligned} A_m &= (\Sigma x_i A_i^{\frac{1}{2}})^2, \\ B_m &= \frac{1}{8} \Sigma x_i x_j (B_i^{\frac{1}{2}} + B_j^{\frac{1}{2}})^2, \\ c_m &= (\Sigma x_i c_i^{\frac{1}{2}})^2, \\ a_m &= \Sigma x_i a_i, \\ b_m &= \Sigma x_i b_i. \end{aligned}$$

The square root combination ( $A_m, c_m$ ) has already been used for the constant  $a$  of Van der Waal's equation of state<sup>10)</sup>. The Lorentz combination ( $B_m$ ) follows from an averaging of molecular diameters

and it has been applied to the constant  $b$  of Van der Waal's equation<sup>11</sup>). The linear combination is applied to both constants  $a_m$  and  $b_m$  respectively.

The approximate solution of  $V$  according to (13) gives

$$V = \sum n_i \frac{RT}{p} + \frac{\sum n_i \beta_m}{RT} + \left( -\frac{\sum n_i \beta_m^2}{(RT)^3} + \frac{\sum n_i \gamma_m}{(RT)^2} \right) p + \\ + \left( \frac{2 \sum n_i \beta_m^3}{(RT)^5} - \frac{3 \sum n_i \beta_m \gamma_m}{(RT)^4} + \frac{\sum n_i \delta_m}{(RT)^3} \right) p^2 + \dots \quad (15)$$

In case of a binary mixture, of course,  $\sum n_i = n = n_1 + n_2$ .

§ 6. *Integration of the equilibrium formula.* By means of the equation of state for a pure gas (13) and that for a gas mixture (15) we can perform the integration of the first two integrals of equation (9); neglecting the compressibility of the condensed nitrogen we get the following relation for the enhancement factor:

$$RT \ln f = - \left[ \frac{\partial}{\partial n_1} \left( \sum n_i \frac{\beta_m}{RT} \right) p + \frac{\partial}{\partial n_1} \left( -\sum n_i \frac{\beta_m^2}{(RT)^3} + \sum n_i \frac{\gamma_m}{(RT)^2} \right) \frac{1}{2} p^2 + \right. \\ \left. + \frac{\partial}{\partial n_1} \left( \sum n_i \frac{2\beta_m^3}{(RT)^5} - \sum n_i \frac{3\beta_m \gamma_m}{(RT)^4} + \sum n_i \frac{\delta_m}{(RT)^3} \right) \frac{1}{6} p^3 \right] + \\ + \frac{\beta_1}{RT} p_{01} + \left( -\frac{\beta_1^2}{(RT)^3} + \frac{\gamma_1}{(RT)^2} \right) \frac{1}{2} p_{01}^2 + \\ + \left( \frac{2\beta_1^3}{(RT)^5} - \frac{3\beta_1 \gamma_1}{(RT)^4} + \frac{\delta_1}{(RT)^3} \right) \frac{1}{6} p_{01}^3 + v_{01} (p - p_{01}). \quad (16)$$

For the sake of simplicity we shall define the quantities  $\beta_{12}$ ,  $\gamma_{12}$  and  $\delta_{12}$  ("interaction coefficients") by means of the following differential quotients:

$$\frac{\partial}{\partial n_1} (\sum n_i \beta_m) = 2\beta_{12} - \beta_2, \\ \frac{\partial}{\partial n_1} (\sum n_i \gamma_m) = 2\gamma_{12} - \gamma_2, \\ \frac{\partial}{\partial n_1} (\sum n_i \delta_m) = 2\delta_{12} - \delta_2. \quad (17)$$

The substitutions (17) enable us to perform the differentiations

in (16); remembering that  $x_1$  is small and  $x_2$  is almost equal to 1, we obtain

$$\begin{aligned}\frac{\partial}{\partial n_1}(\Sigma n_i \beta_m^2) &= \beta_m^2 + 2\beta_m \Sigma n_i \frac{\partial \beta_m}{\partial n_1} = \beta_m^2 + 2\beta_2(2\beta_{12} - 2\beta_2) = 4\beta_{12}\beta_2 - 3\beta_2^2, \\ \frac{\partial}{\partial n_1}(\Sigma n_i 2\beta_m^3) &= 12\beta_2^2\beta_{12} - 10\beta_2^3, \\ \frac{\partial}{\partial n_1}(\Sigma n_i 3\beta_m \gamma_m) &= 6(\gamma_2\beta_{12} + \beta_2\gamma_{12}) - 9\gamma_2\beta_2.\end{aligned}\quad (18)$$

As the terms of (16) containing the vapour pressure of the condensed nitrogen are negligible we shall omit them; by using the definitions (17) and the relations (18) we can write down (16) as a series in ascending powers of the total pressure  $p$ :

$$\begin{aligned}\ln f &= \left(\frac{v_{01}}{RT} - \frac{2\beta_{12} - \beta_2}{(RT)^2}\right)p + \\ &+ \left(\frac{4\beta_{12}\beta_2 - 3\beta_2^2}{2(RT)^4} - \frac{2\gamma_{12} - \gamma_2}{2(RT)^3}\right)p^2 + \\ &+ \left(-\frac{12\beta_2^2\beta_{12} - 10\beta_2^3}{3(RT)^6} + \frac{6(\gamma_2\beta_{12} + \gamma_{12}\beta_2) - 9\gamma_2\beta_2}{3(RT)^5} - \frac{2\delta_{12} - \delta_2}{3(RT)^4}\right)p^3.\end{aligned}\quad (19)$$

The parameters  $\beta_{12}$ ,  $\gamma_{12}$  and  $\delta_{12}$  are calculated in the subsequent section.

§7. *Calculation of the coefficients for the  $H_2$ - $N_2$  mixture in the equation of state.* The laborious work involving the calculation of the parameters  $\beta_{12}$ ,  $\gamma_{12}$ ,  $\delta_{12}$  may be simplified by the introduction of the following abbreviations:

$$\begin{aligned}B_{12} &= \frac{1}{8}(B_1^\dagger + B_2^\dagger)^3, & a_{12} &= \frac{1}{2}(a_1 + a_2), \\ A_{12} &= A_1^\dagger A_2^\dagger, & b_{12} &= \frac{1}{2}(b_1 + b_2), \\ c_{12} &= c_1^\dagger c_2^\dagger.\end{aligned}\quad (20)$$

With respect to the combination rules (14) and the relations  $x_1 \approx 0$ ,  $x_2 \approx 1$ , we get

$$\begin{aligned}n \frac{\partial B_m}{\partial n_1} &= n \frac{\partial}{\partial n_1} \frac{1}{8} \left[ \Sigma \frac{n_i n_j}{n^2} (B_i^\dagger + B_j^\dagger)^3 \right] \\ &= n \frac{2n_1 B_1 + 2n_2 B_{12}}{n^2} - n \frac{2(n_1^2 B_1 + 2n_1 n_2 B_{12} + n_2^2 B_2)}{n^3} \\ &= 2x_1 B_1 + 2x_2 B_{12} - 2B_2 = 2B_{12} - 2B_2,\end{aligned}$$

$$\begin{aligned} n \frac{\partial A_m}{\partial n_1} &= n \frac{\partial}{\partial n_1} \left( \frac{n_1 A_1^{\frac{1}{2}} + n_2 A_2^{\frac{1}{2}}}{n} \right)^2 \\ &= 2n \frac{n_1 A_1^{\frac{1}{2}} + n_2 A_2^{\frac{1}{2}}}{n} \frac{\partial}{\partial n_1} \left( \frac{n_1 A_1^{\frac{1}{2}} + n_2 A_2^{\frac{1}{2}}}{n} \right) \\ &= 2(x_1 A_1^{\frac{1}{2}} + x_2 A_2^{\frac{1}{2}}) (A_1^{\frac{1}{2}} - x_1 A_1^{\frac{1}{2}} - x_2 A_2^{\frac{1}{2}}) = 2A_1^{\frac{1}{2}} A_2^{\frac{1}{2}} - 2A_2 = 2A_{12} - 2A_2, \end{aligned}$$

$$n \frac{\partial c_m}{\partial n_1} = 2c_{12} - 2c_2,$$

$$n \frac{\partial a_m}{\partial n_1} = n \frac{\partial}{\partial n_1} \left( \frac{n_1 a_1 + n_2 a_2}{n} \right) = a_1 - x_1 a_1 - x_2 a_2 = a_1 - a_2 = 2a_{12} - 2a_2,$$

$$n \frac{\partial b_m}{\partial n_1} = 2b_{12} - 2b_2.$$

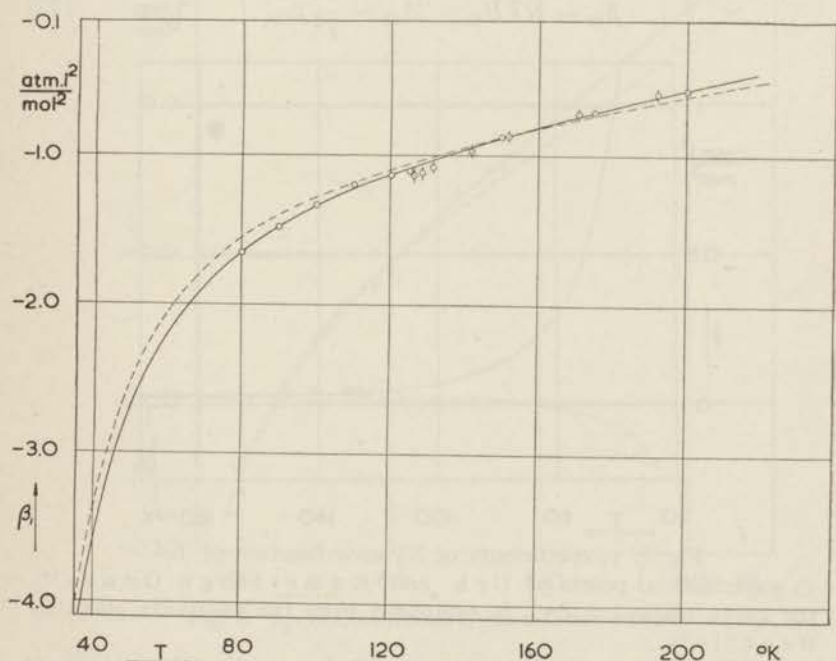


Fig. 6.  $\beta_1$ -coefficients of  $N_2$  as a function of  $T$ .

- ⊙ experimental points of Urk and Kamerlingh Onnes<sup>12)</sup>,
- ⊙ points tabulated by White<sup>13)</sup>,
- the curve marked - - - - is computed from the constants given by Beattie<sup>7)</sup>,
- the curve marked ——— is computed from the constants (27).

We can now perform the differentiation involving the calculation of the interaction coefficient  $\beta_{12}$  given by (17) with respect to the combination rules (14):

$$\begin{aligned} \frac{\partial}{\partial n_1} (\Sigma n_i \beta_m) &= \beta_m + n \frac{\partial \beta_m}{\partial n_1} = \beta_m + n \frac{\partial}{\partial n_1} \left( RTB_m - A_m - \frac{R}{T^2} c_m \right) \\ &= \beta_2 + RT(2B_{12} - 2B_2) - (2A_{12} - 2A_2) - \frac{R}{T^2} (2c_{12} - 2c_2) \\ &= \beta_2 + 2 \left( RTB_{12} - A_{12} - \frac{R}{T^2} c_{12} \right) - 2 \left( RTB_2 - A_2 - \frac{R}{T^2} c_2 \right) \quad (21) \\ &= 2 \left( RTB_{12} - A_{12} - \frac{R}{T^2} c_{12} \right) - \beta_2. \end{aligned}$$

Thus we find

$$\beta_{12} = RTB_{12} - A_{12} - \frac{R}{T^2} c_{12}. \quad (22)$$

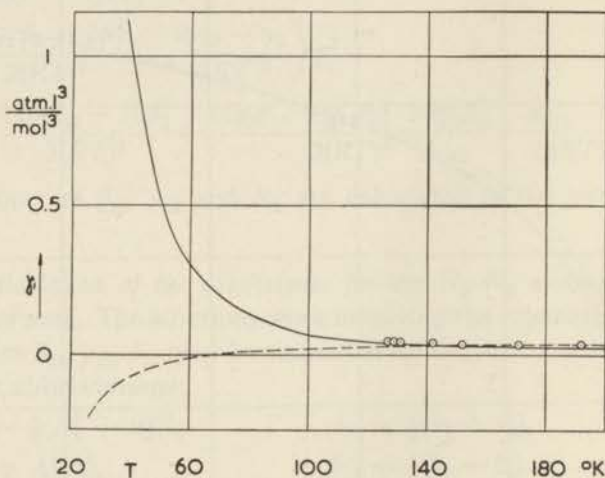


Fig. 7.  $\gamma_1$ -coefficients of  $N_2$  as a function of  $T$ .

○ experimental points of Urk and Kamerlingh Onnes<sup>12</sup>, the curve marked - - - is computed from the constants given by Beattie<sup>7</sup>, the curve marked — is extrapolated according to values of White<sup>13</sup>.

Similarly the calculation of  $\gamma_{12}$  results in an analogous relation:

$$\frac{\partial}{\partial n_1} (\Sigma n_i \gamma_m) = \gamma_m + n \frac{\partial}{\partial n_1} (-RTB_m b_m + A_m a_m - RB_m c_m / T^2)$$

$$\begin{aligned}
 &= \gamma_m - RT(2B_{12} - 2B_2) b_2 - RTB_2 (2b_{12} - 2b_2) + \\
 &\quad + (2A_{12} - 2A_2) a_2 - A_2 (2a_{12} - 2a_2) - \\
 &\quad - (R/T^2) (2B_{12} - 2B_2) c_2 - (R/T^2) B_2 (2c_{12} - 2c_2) \\
 &= \gamma_2 + 2(-RTB_{12}b_2 + A_{12}a_2 - RB_{12}c_2/T^2 - \\
 &\quad - RTB_2b_{12} + A_2a_{12} - RB_2c_{12}/T^2) - 4(-RTB_2b_2 + A_2a_2 - RB_2c_2/T^2) \\
 &= \gamma_2 + 2\Gamma_{12} - 4\gamma_2. \tag{23}
 \end{aligned}$$

By (23) the quantity  $\Gamma_{12}$  is defined.

The comparison of (23) with (17) gives

$$\begin{aligned}
 \gamma_{12} = \Gamma_{12} - \gamma_2, \Gamma_{12} = &-RTB_{12}b_2 + A_{12}a_2 - RB_{12}c_2/T^2 + \\
 &-RTB_2b_{12} + A_2a_{12} - RB_2c_{12}/T^2. \tag{24}
 \end{aligned}$$

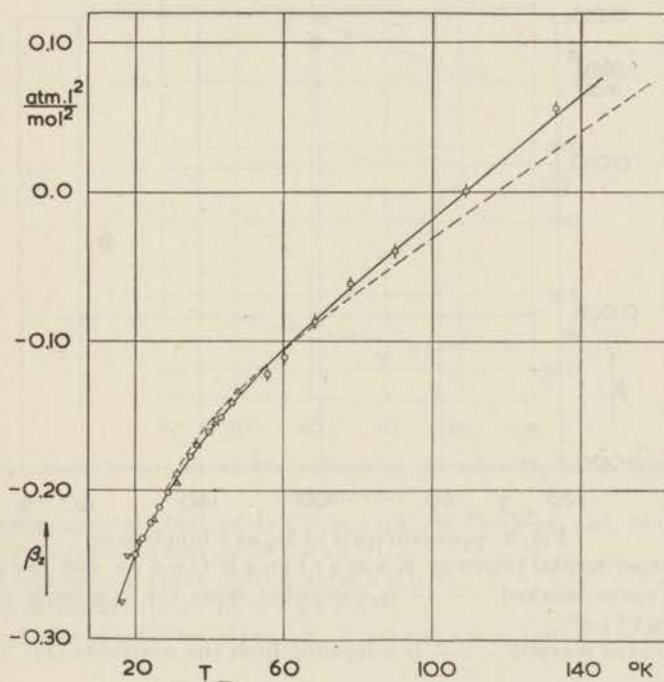


Fig. 8.  $\beta_2$ -coefficients of  $H_2$  as a function of  $T$ .

- experimental points of Kamerlingh Onnes and Braak<sup>14</sup>,
  - △ experimental points of Nijhoff and Keesom<sup>15</sup>,
  - ⊙ experimental points of Schäfer<sup>16</sup>,
  - ▽ experimental points of Kamerlingh Onnes and De Haas<sup>17</sup>,
- the curve marked - - - - is computed from the constants given by Beattie<sup>7</sup>,
- the curve marked ——— is computed from the constants (28).

The determination of the coefficient  $\delta_{12}$  is achieved by the same method:

$$\begin{aligned} \frac{\partial}{\partial n_1} (\Sigma n_i \delta_m) &= \delta_m + n \frac{\partial}{\partial n_1} (RB_m b_m c_m / T^2) = \\ &= \delta_m + (R/T^2) [b_2 c_2 (2B_{12} - 2B_2) + B_2 c_2 (2b_{12} - 2b_2) + \\ &\quad + B_2 c_2 (2c_{12} - 2c_2)] = \\ &= \delta_2 + (2R/T^2) (B_{12} b_2 c_2 + B_2 b_{12} c_2 + B_2 b_2 c_{12}) - \\ &\quad - 6RB_2 b_2 c_2 / T^2 \\ &= \delta_2 + 2\Delta_{12} - 6\delta_2, \end{aligned} \quad (25)$$

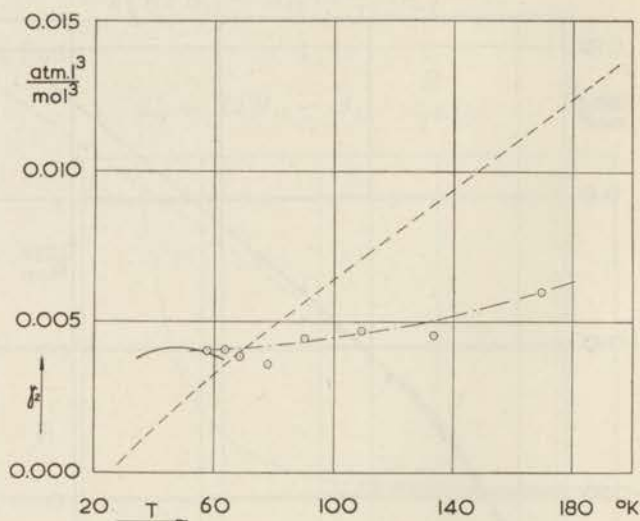


Fig. 9.  $\gamma_2$ -coefficients of  $H_2$  as a function of  $T$ .

⊙ experimental points of Kamerlingh Onnes and Braak<sup>14</sup>), the curve marked - - - is computed from the constants given by Beattie<sup>7</sup>),

the curve marked — is computed from the constants (28).

where the quantity  $\Delta_{12}$  is introduced.

The comparison of (25) with (17) gives

$$\begin{aligned} \delta_{12} &= \Delta_{12} - 2\delta_2, \\ \Delta_{12} &= (R/T^2) (B_{12} b_2 c_2 + B_2 b_{12} c_2 + B_2 b_2 c_{12}). \end{aligned} \quad (26)$$

The substitutions of (22), (24) and (26) into (19) and the adjustment of the corresponding constants of the equation of state for pure

hydrogen and nitrogen enable us to evaluate numerically the enhancement factor  $f$ .

§ 8. *Numerical evaluation of the linear theory.* The formula (19) for the enhancement factor  $f(p, T)$  is given in the form of an expansion in powers of the pressure; the linear term requires the knowledge of the second virial coefficient, the quadratic term contains the third virial coefficient and the cubic term depends on the fourth virial

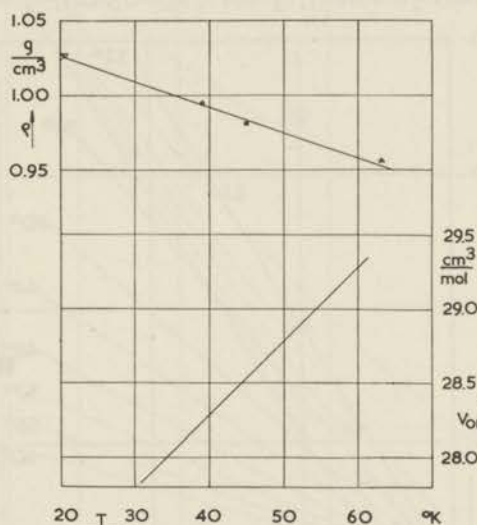


Fig. 10. Density  $\rho$  and molar volume  $v_{01}$  of solid  $N_2$  as a function of temperature.

- experimental point of De Smedt, Keesom and Mooy<sup>18</sup>),
- ▽ experimental point of Dewar<sup>19</sup>),
- ◇ experimental point of Ruhemann<sup>20</sup>),
- experimental point of Vegard<sup>21</sup>),
- △ calculated point by Simon, Ruhemann and Edwards<sup>22</sup>).

coefficient of the constituent components of the mixture, *i.e.*, in our case, the hydrogen-nitrogen mixture. We shall first limit the calculations to the evaluation of the linear term. This case will be referred to as the "linear  $p, T$ -theory" in contrast to the quadratic or cubic  $p, T$ -theory; both the latter approximations and the  $V, T$ -theory in  $V, T$ -variables will be discussed later in chapter V.

The  $\beta_1$ - and  $\gamma_1$ -virial coefficients are extrapolated in fig. 6 and 7 from the known experimental points for pure nitrogen. We adjusted

the Beattie-Bridgeman coefficients for temperatures between 60°K and 32°K and for pressures up to 50 atm; all of them are given in atm-liter-deg-mole system:

$$A_1 = 1.491, B_1 = 0.0625, c_1 = 44350, a_1 = 1.22, b_1 = 322. \quad (27)$$

The interpolation of the measurements of  $\beta_2$  and  $\gamma_2$  virial coefficients of hydrogen (see fig. 8 and 9) results in the following adjusted constants of the equation of state:

$$A_2 = 0.2233, B_2 = 0.0251, c_2 = 379, a_2 = 0.0229, b_2 = 0.00652. \quad (28)$$

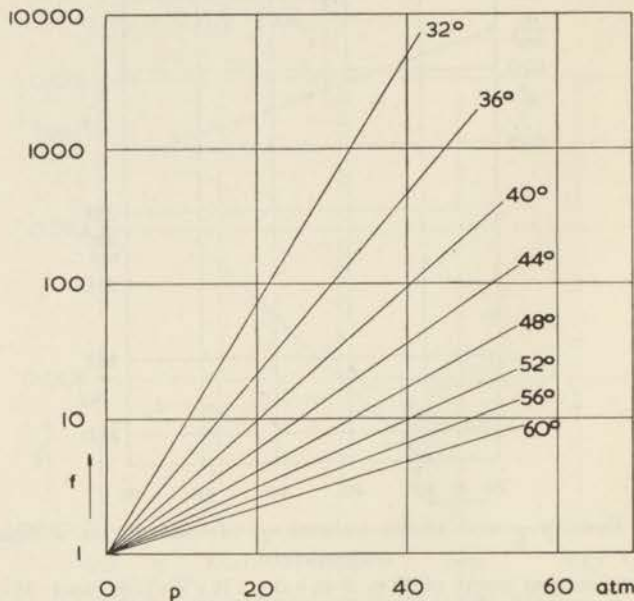


Fig. 11. Enhancement factor  $f$  computed from the linear  $p, T$ -theory.

The molar volume of the solid nitrogen is shown in fig. 10 as a function of temperature; according to these values the density was assumed to be a linear function between 20°K and 60°K. The compressibility of the solid phase was neglected.

The vapour pressure of pure solid nitrogen  $p_{01}$  was taken from the report of National Bureau of Standards<sup>3)</sup>.

It has not been considered necessary to reproduce the numerous intermediate series of calculated data when proceeding according to the general computation scheme developed in previous sections. The numerical results of the linear theory are represented in the

figs. 11, 12 and 13. The logarithms of the enhancement factor were calculated in 4 degK-intervals from 60°K and 32°K at pressures of 50, 25, 15, 10, 5 and 1.3 atm;  $\ln f$  plotted against the pressure gives, of course, a set of corresponding straight lines (see fig. 11).

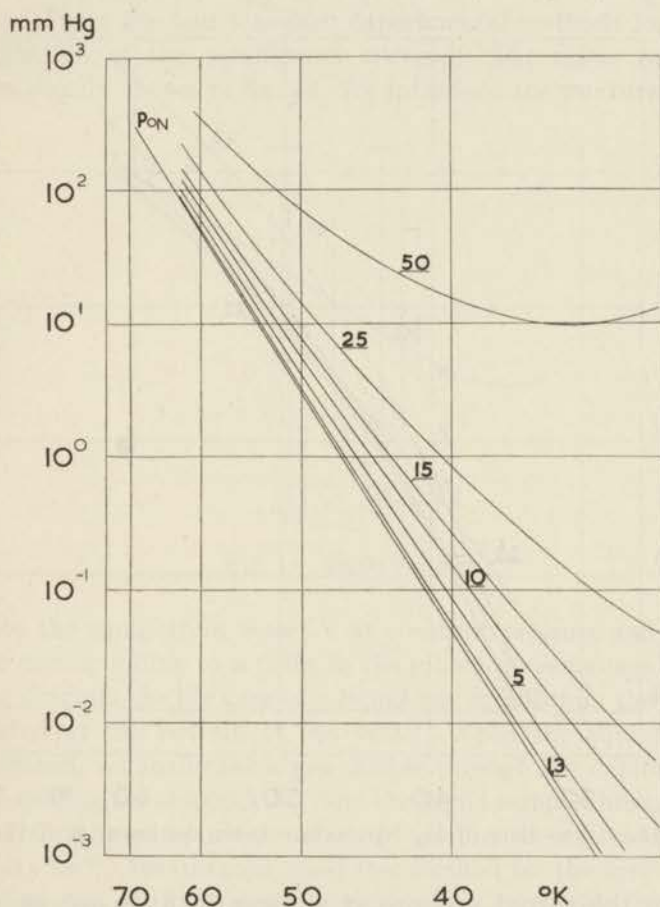


Fig. 12. Partial pressure of  $N_2$  in  $H_2$  from the linear  $p, T$ -theory.

Considering the quantitative values of  $f$  we can expect, therefore, an appreciable increase of the partial pressure of nitrogen in hydrogen as a consequence of the physical interpretation of (10). This quantity  $p x_1$  is shown as a function of the reciprocal of temperature in fig. 12. In the same diagram we added for comparison the vapour pressure curve of pure solid nitrogen; if one assumes the ideal character of

the gas mixture, the curves for any value of the total pressure  $p$  will be expected in the vicinity of the vapour pressure curve of pure solid nitrogen because of the relatively small hydrostatic effect still existing.

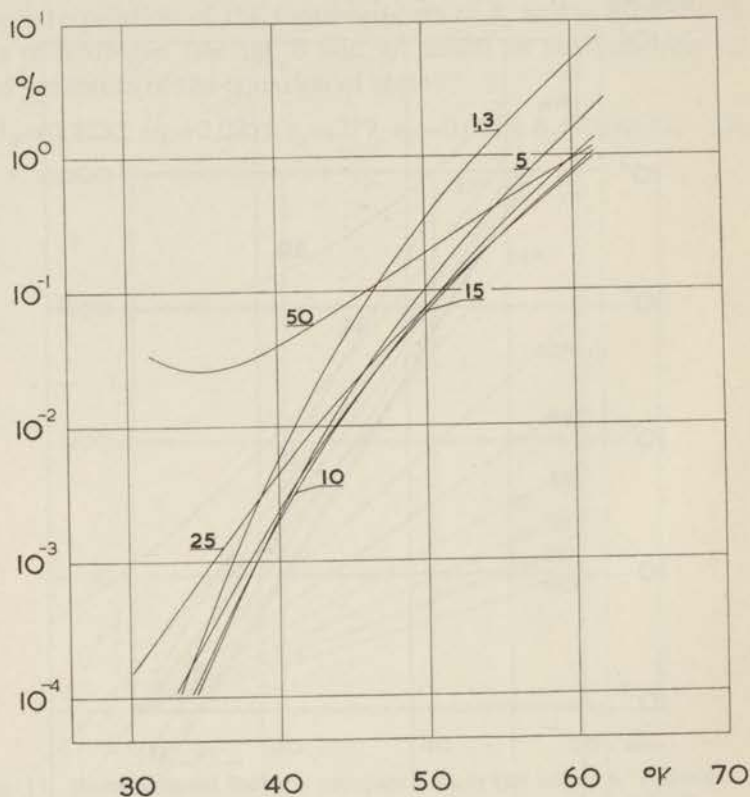


Fig. 13.  $x$ ,  $T$ -isobars of  $H_2$ - $N_2$ -mixture from the linear  $p$ ,  $T$ -theory.

From the partial pressure of nitrogen in hydrogen we finally calculated the concentration of the gas phase as a function of the temperature (see fig. 13). We shall later see that this linear  $p$ ,  $T$ -theory satisfactorily approximates the actual behaviour of the binary system  $H_2$ - $N_2$ . The area of agreement, however, will be limited to higher temperatures and lower pressures.

CHAPTER III. EXPERIMENTAL DETERMINATION OF EQUILIBRIUM CURVES

§ 9. *Experimental methods for the determination of the equilibrium curves.* There are four standard experimental methods for the determination of the equilibrium curves<sup>5)</sup>. The static method is schematically shown in fig. 14. We introduce the mixture through

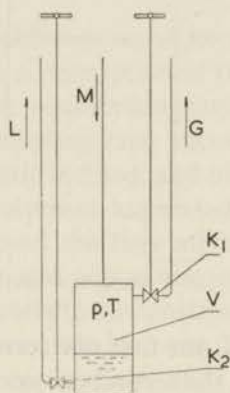


Fig. 14. Static method.

M into the equilibrium vessel V at constant pressure and temperature corresponding to a point in the inhomogeneous region of the phase diagram. In the case of a liquid-gas equilibrium the liquid is collected at the bottom of the vessel. When the equilibrium is established, we shall take a gas sample through the capillary tube G by opening the stopcock  $K_1$ , and the liquid sample through L and  $K_2$ . Then the composition of both samples is analysed. Ver-schöyle<sup>2)</sup>, for instance, used this method for the investigation of mixtures of hydrogen-nitrogen-carbon monoxide at higher temperatures.

The volumetric method has been developed by K u e n e n<sup>5)</sup> at Leiden. Here we do not need to analyse any samples. We start with a known composition of the mixture stored in the container F in fig. 15. We fill the section of the apparatus between the stopcocks  $K_1$ ,  $K_2$ . The volume of this part, consisting mainly of the volume of the Bourdon gauge  $M_1$ , is of the same order of magnitude as the volume of the second Bourdon gauge  $M_2$ . The equilibrium vessel V

is kept at the temperature  $T$ , and the gas is then transferred in small portions through the valve  $K_2$  and the pressure of  $M_2$  is plotted as a function of the pressure read on  $M_1$ . We shall observe then two more

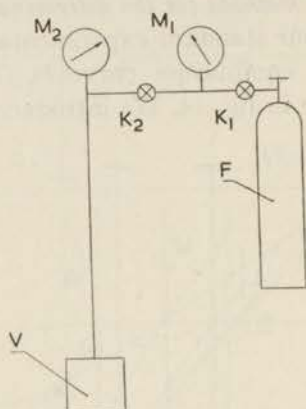


Fig. 15. Volumetric method.

or less pronounced kinks: the first one corresponds to the beginning of the condensation and the second one occurs at the moment when the equilibrium vessel is completely filled with the condensed phase.

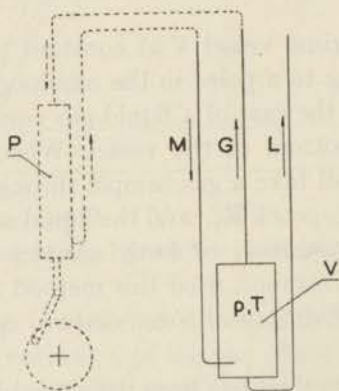


Fig. 16. Dynamic methods.

Verschyle<sup>2)</sup> also has applied this method for his work on the hydrogen-nitrogen-carbon monoxide-mixtures.

In fig. 16 a sketch is given of the flow method (full lines) and of the circulation method (dotted lines). The mixture is passed continuously

at a constant pressure through the capillary tube M to the equilibrium vessel kept at the temperature T. The gaseous phase flows out of the cryostat through G and is to be analysed. In the case of a liquid phase its composition may be determined by sampling a portion of the liquid through L. The application of the circulation method implies the reintroduction of the gas phase into the equilibrium vessel by means of the mercury-column circulating pump; both phases are then subsequently analysed until the tests give consistent results.

§ 10. *Cryostat and equilibrium vessel for the flow method.* In the previous section we gave a description of the different methods for the determination of the equilibrium curves. Owing to the difficulties in making the sampling taps vacuum-tight at low temperatures when using the static method, and owing to the rather elaborate and complicated equipment associated with the volumetric or circulation method we used the flow method. Moreover, the flow method comes closer to the actual use of the resulting data in technical applications, namely in the construction of heat-exchangers. If properly handled it was reliable even for low pressures where other methods are less appropriate, and gave us quite accurate results.

In fig. 17 a sketch is given of our cryostat. The mixture from the storage cylinder F is passed through a copper capillary tube of 4 mm outer diameter and 3 mm inner diameter to the equilibrium vessel V. The mixture entering the reservoir is directed so as to strike a large number of plates which increase the surface of contact and give the solid a good chance for depositing thereupon. This equilibrium vessel (of about 60 cm<sup>3</sup>) is made of copper and has a sufficient heat capacity to eliminate the possible temperature fluctuations; the temperature difference between the top and the bottom of the equilibrium vessel measured by means of two thermocouples proved to be negligible.

During the run the pressure is maintained constant by regulating the high pressure tap S<sub>1</sub>; when the tap S<sub>2</sub> (or S<sub>3</sub>) is opened and S<sub>3</sub> (or S<sub>2</sub>) is closed, we can read the pressure in the inlet (or outlet) tube T<sub>1</sub> (or T<sub>2</sub>) on the Bourdon gauge which had been previously calibrated. The high pressure is then reduced in the tap S<sub>4</sub>, and the vapour phase is passed continuously through the safety valve S into the atmosphere. When it may be assumed that a stationary state has

been reached, the sample of the vapour to be analysed is passed through the valve  $S_6$  at the end of the run. The pressure is kept constant during the operation. Experiments were done at different flow velocities.

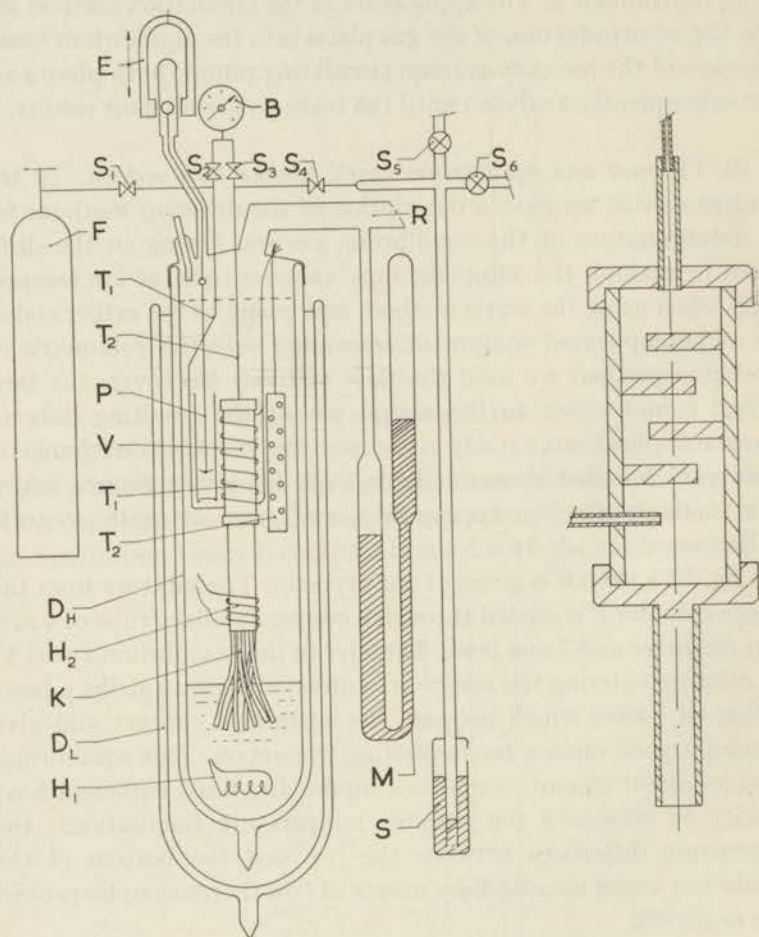


Fig. 17. Cryostat with equilibrium vessel.

The cryostat cap is fitted with a vacuum connection R; by pumping off a bath of liquid oxygen in the Dewar vessel  $D_H$  through R we can reach temperatures down to about  $56^\circ\text{K}$ . The outer Dewar vessel  $D_L$  was filled with liquid air. The mechanical pump stirrer P was operated by means of the electromagnet E. The actual temper-

ature of the equilibrium vessel was measured with the aid of two resistance thermometers; the platinum thermometer  $T_2$  had been calibrated against the Leiden standard resistance thermometer Pt 68; the lead wire  $T_1$  was wound around the equilibrium vessel and was compared with the platinum thermometer  $T_2$ . Both thermometers were subsequently checked against the accurately known vapour pressure of oxygen; we found that both resistances remained satisfactorily constant.

The pressure of the oxygen bath was indicated by the mercury manometer M. It appeared to be difficult to attain the triple point of oxygen or the eutectic temperature ( $50.1^\circ\text{K}$ ) of the mixture oxygen-nitrogen, because the vapour pressure at the quadruple eutectic point is only 1.2 mm Hg and, therefore, the cooling down periods are very long. Already for the above mentioned  $56^\circ\text{K}$  (corresponding pressure = 2.0 mm Hg) it took us about an hour before a stationary temperature was reached. As we had no pump of large capacity at our disposal to maintain such low pressure over a large quantity of liquid, we used the hydrogen gas cryostat as described below.

For the measurements at temperatures below  $56^\circ\text{K}$  down to  $30^\circ\text{K}$  we took instead of a Dewar vessel  $D_H$  another much longer one, filled with liquid hydrogen up to approximately one third of its length. The equilibrium vessel was then connected with the low level of liquid hydrogen through a German silver tube G and a bundle of cotton cords K. The heat conduction of the metals and the cold stream of hydrogen vapour cooled down the equilibrium vessel. If both heaters  $H_1$  and  $H_2$  were properly operated, it was not difficult to maintain a constant temperature within few tenths of a degree during the run of half an hour, or longer when necessary. It made no difference for the temperatures between  $58^\circ\text{K}$  and  $52^\circ\text{K}$  whether we worked with a liquid oxygen bath (or  $\text{O}_2\text{-N}_2$ -bath) or with a hydrogen vapour cryostat; we got just the same results in both cases.

§ 11. *Apparatus for analysis of a binary gas mixture.* According to the theoretical calculations given in chapter II, the concentrations of nitrogen in the gas phase were expected to decrease rapidly with decreasing temperature; indeed, it was found from the first preliminary measurements that we could not easily determine the composition of the gas samples by the classical methods of gas

analysis, because the concentration of nitrogen became of the order of magnitude of 0.1% already at the temperature of 50°K. Therefore, we decided to develop a physical method to analyse the mixture, and as had been expected, much of our research time was spent in perfecting our analysis system until we could succeed in measuring very small condensable impurities of hydrogen down to about 0.00002%. These small quantities of N<sub>2</sub> (or of CO, or of N<sub>2</sub> + CO) were frozen out at 20°K in liquid hydrogen, which implies that the partial pressure of nitrogen virtually disappears at this temperature. It is very easy to calculate then the concentration from the decrease of the total pressure of the mixture concerned.

The known quantity of the gas mixture had to flow through a capillary where the solidification of the condensable impurities took place. In our first apparatus we intended to use a mechanical piston pump for the circulation of the gas, but we did not succeed in achieving a vacuum-tight system.

Thus we abandoned the mechanical pump system and designed for the same purpose a special mercury circulating pump based on the alternating displacement of mercury in two  $\frac{1}{2}$  l containers fixed on a swinging pendulum. This device of glass was connected by metal (later rubber and plastic) flexible tubes with the circulating circuit which was at first entirely made of copper except for the manometer gauges (glass). The system was evacuated by means of a rotary oil pump, and later the vacuum was improved by a char coal trap at the temperature of liquid air. The main difficulty of such a system was the degassing of the long copper tubes; subsequently the porosity of the flexible rubber or plastic connections caused us much trouble.

We therefore constructed a new system composed entirely of glass; we replaced the above mentioned type of mercury pump by a double mercury-column circulating pump; and we used the mercury diffusion pump for evacuation of the whole analytical apparatus. The sketch of the complete assembly is given in fig. 18. The diffusion pump was connected to the system at V; during the evacuation period the vapour passes from the equilibrium vessel through S (fig. 17) out into the atmosphere, the stopcock S<sub>6</sub> being closed. When the equilibrium is reached, the stopcocks S<sub>7</sub>, S<sub>12</sub>, S<sub>14</sub>, S<sub>17</sub>, S<sub>18</sub>, S<sub>19</sub>, S<sub>20</sub>, are closed, and the system is filled with the sample through S<sub>6</sub> and S<sub>8</sub> up to a certain pressure depending upon the expected concentration. The samples may, of course, be stored in the balloons B<sub>1</sub>, B<sub>2</sub>, or B<sub>3</sub>.

The three-way stopcock  $S_8$  is then closed, and both mercury columns are adjusted to the fixed mark  $M$ ; the total pressure  $p$  is read on the mercury manometer  $M_1$ . The stopcocks  $S_{13}$  and  $S_9$  are closed, the cryostat is filled with liquid hydrogen  $H$ , and by means of the double mercury-column pump (*i.e.*, by proper manipulation of both clamps  $C_1$  and  $C_2$  when displacing the mercury level) and by means of the commutation four-way stopcock  $S_{10}$  one can circulate the mixture

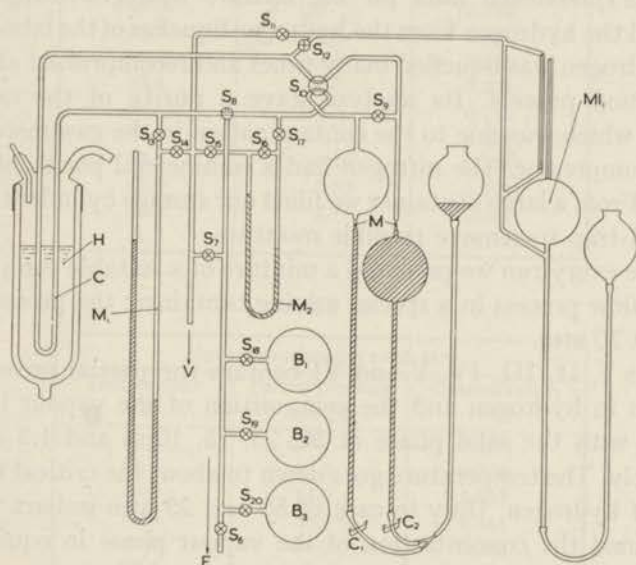


Fig. 18. Analytical apparatus for  $H_2-N_2$ -gas mixture.

always in the same direction through the capillary  $C$ , where  $N_2$  (or  $CO$  or both of them) remains condensed with zero partial pressure. The whole system is again evacuated through  $S_{13}$  and  $S_{14}$ , the four-way stopcock  $S_{10}$  is set in the neutral position so as to separate the large volume of the pump ( $= 488 \text{ cm}^3$ ) from the remaining part ( $= 42.9 \text{ cm}^3$ ). When the stopcocks  $S_{13}$ ,  $S_{15}$ ,  $S_{16}$  are closed and  $S_{17}$  is opened, the liquid hydrogen is removed; the gaseous  $N_2$  (or  $CO$  or both of them) expands into the small volume; the pressure  $\Delta p$  is read on the differential manometer  $M_2$ , filled with octoil-S. In the case of concentrations below  $0.05\%$  we let the gas expand through  $S_{12}$  into the MacLeod gauge  $MI_1$ . From the calibrated volumes of distinct parts of the system, the known density of mercury and

octoil-S, and the pressures  $p$  and  $\Delta p$  we can easily calculate the concentration,  $c = C \Delta p/p\%$ , where  $C$  is a constant depending on the geometry of the system.

#### CHAPTER IV. EXPERIMENTAL RESULTS OF THE SYSTEMS HYDROGEN-NITROGEN AND HYDROGEN-CARBON MONOXIDE

§ 12. *Experimental data for the mixture hydrogen-nitrogen.* We obtained the hydrogen from the hydrogen liquefier of the laboratory. This hydrogen was liquefied many times and recompressed after the liquefaction process. Its analysis gave a purity of the order of 99.90% which was due to the contamination in the gasometers and in the compressor. The nitrogen had a commercial purity of about 99.8%. From a large container we filled our storage cylinder through a NaOH-trap to remove possible moisture.

Before every run we prepared a mixture of a suitable composition for the flow process in a special mixing container; the pressure was of about 70 atm.

Tables I, II, III, IV, V and VI contain the partial pressures of nitrogen in hydrogen and the composition of the vapour in equilibrium with the solid phase at 50, 25, 15, 10, 5 and 1.3 atm respectively. The temperature goes down to about the critical temperature of hydrogen. Only in case of 50 and 25 atm-isobars we also determined the concentration of the vapour phase in equilibrium with the liquid phase.

TABLE I

Hydrogen-nitrogen isobar at 50 atm		
Temperature °K	Partial pressure mm Hg	Concentration %
70.4	1210	3.18
69.6	1140	3.01
68.6	1080	2.86
64.9	695	1.83
60.2	425	1.12
55.2	250	0.658
55.1	236	0.620
47.2	82.9	0.218
35.1	16.7	0.044
25.1	6.8	0.018
25.1	6.1	0.016

TABLE II

Hydrogen-nitrogen isobar at 25 atm		
Temperature °K	Partial pressure mm Hg	Concentration %
69.4	628	3.30
65.5	330	1.73
65.2	326	1.72
60.3	143	0.753
59.9	137	0.722
59.9	137	0.723
56.4	65.6	0.346
56.2	67.5	0.356
53.4	38.7	0.204
53.4	35.3	0.186
44.3	4.15	0.0219
42.1	3.16	0.0167
38.9	2.50	0.0131
33.2	2.11	0.0111
31.7	1.70	0.00899

TABLE III

Hydrogen-nitrogen at 15 atm		
Temperature °K	Partial pressure mm Hg	Concentration %
62.3	133	1.17
60.0	88.6	0.778
59.0	64.6	0.567
57.4	50.4	0.441
55.0	34.0	0.298
50.1	7.40	0.065
43.9	1.26	0.0111
38.0	0.211	0.00185
36.1	0.150	0.00132
34.6	0.125	0.00110
32.1	0.137	0.00120

The experimental points of the vapour pressure of pure nitrogen do not cover our complete temperature range and, therefore, we approximately determined some vapour pressure values by connecting our analytical system with the equilibrium vessel; these data are given in table VII.

§ 13. *Experimental data of the mixture hydrogen-carbon monoxide.*  
For the production of the first quantity of carbon monoxide we used nickelcarbonyl,  $\text{Ni}(\text{CO})_4$ , which splits into one mole of metallic Ni

TABLE IV

Hydrogen-nitrogen isobar at 10 atm		
Temperature °K	Partial pressure mm Hg	Concentration %
61.8	102	1.34
60.4	74.3	0.977
58.2	47.3	0.630
56.6	33.6	0.443
54.8	24.0	0.316
50.2	6.15	0.0809
42.2	0.455	0.00558
38.2	0.0848	0.00112
34.7	0.0316	0.000416
31.9	0.0139	0.000183
29.8	0.00900	0.000118
29.6	0.00885	0.000117

TABLE V

Hydrogen-nitrogen isobar at 5 atm		
Temperature °K	Partial pressure mm Hg	Concentration %
60.9	71.5	1.88
60.8	63.2	1.67
57.8	34.2	0.902
56.7	26.0	0.685
54.8	18.3	0.482
50.2	5.40	0.142
42.4	0.300	0.00790
38.1	0.0316	0.000832
34.9	0.00625	0.000164
31.6	0.00322	0.0000846
30.2	0.00288	0.0000758
28.0	0.00219	0.0000577

TABLE VI

Hydrogen-nitrogen isobar at 1.3 atm		
Temperature °K	Partial pressure mm Hg	Concentration %
60.1	59.5	6.04
59.2	40.0	4.05
58.0	29.0	2.93
49.1	2.08	0.211
45.3	0.530	0.0537
39.1	0.0334	0.00339
35.9	0.00707	0.000717
34.1	0.00198	0.000201



In the tables VIII, IX, X, XI, XII and XIII we gathered the values of the vapour pressure of the carbon monoxide in hydrogen,

TABLE VIII

Hydrogen-carbon monoxide isobar at 50 atm		
Temperature °K	Partial pressure mm Hg	Concentration %
69.9	695	1.86
65.7	392	1.03
60.8	190	0.569
57.9	120	0.330
55.4	65.0	0.171
49.7	23.6	0.0623
45.6	12.5	0.0820
35.6	4.67	0.0124

TABLE IX

Hydrogen-carbon monoxide isobar at 25 atm		
Temperature °K	Partial pressure mm Hg	Concentration %
67.7	258	1.36
66.5	191	1.038
62.8	97.9	0.515
60.0	54.0	0.284
56.0	18.7	0.0983
50.4	5.39	0.0234
41.7	2.40	0.0126
35.5	1.61	0.00850

TABLE X

Hydrogen-carbon monoxide isobar at 15 atm		
Temperature °K	Partial pressure mm Hg	Concentration %
60.7	45.7	0.400
59.4	30.3	0.266
55.6	11.8	0.104
54.6	9.50	0.0834
51.4	3.74	0.0328
46.1	0.720	0.00624
44.9	0.348	0.00480
42.5	0.426	0.00374
42.5	0.408	0.00358
42.1	0.365	0.00320
38.1	0.139	0.00139
35.0	0.128	0.00112
34.1	0.117	0.00102
34.1	0.117	0.00103

and the composition of the vapour phase in equilibrium with the solid phase at 50, 25, 15, 10, 5 and 1.3 atm respectively. The temper-

TABLE XI

Hydrogen-carbon monoxide isobar at 10 atm		
Temperature °K	Partial pressure mm Hg	Concentration %
63.0	58.0	0.763
56.2	11.5	0.152
54.2	5.95	0.0784
51.4	3.24	0.0427
51.4	3.24	0.0430
45.8	0.460	0.00605
42.1	0.239	0.00314
37.0	0.0397	0.000522
36.0	0.0270	0.000356
33.9	0.0130	0.000172
31.9	0.00663	0.0000873

TABLE XII

Hydrogen-carbon monoxide isobar at 5 atm		
Temperature °K	Partial pressure mm Hg	Concentration %
62.6	46.5	1.22
56.4	8.89	0.234
54.7	4.30	0.120
51.4	2.08	0.0549
46.2	0.291	0.00765
42.2	0.121	0.00320
37.6	0.0210	0.000552
35.8	0.0137	0.000362
33.4	0.00351	0.0000925

TABLE XIII

Hydrogen-carbon monoxide isobar at 1.3 atm		
Temperautre °K	Partial pressure mm Hg	Concentration %
58.8	12.35	1.25
55.3	5.20	0.527
50.5	1.02	0.103
47.2	0.440	0.0445
44.2	0.165	0.0167
39.8	0.0356	0.00361
38.2	0.0143	0.00145
36.4	0.00612	0.00620
34.4	0.00284	0.000288
32.3	0.00156	0.000158

ature interval ranges from the triple point of carbon monoxide down to about the critical temperature of hydrogen.

§ 14. *Sources of error.* The accuracy of the results depends upon the approach to true equilibrium; a second source of error is the analytical determination of the composition.

The pressure could be regulated accurately within 0.2 atmosphere, and the temperature variations of the equilibrium vessel in the hydrogen gas cryostat in the region between 50°K and 30°K were less than 0.2 degK. Two other parameters which may affect the flow process are the flow velocity and the duration of the run. To check it we started at the same pressure and temperature, and before taking off the gas sample we waited two or three times longer than we did normally. The analysis tests proved it to be sufficient to wait as long as it took for one molecule to pass the system completely with the corresponding known velocity; this was varied between 1 l/min and  $\frac{1}{3}$  l/min without any noticeable effect on the resulting concentration.

To test our analysis method for a binary mixture we successively varied the following parameters: the starting pressure of the sample, the time that was spent on pumping away the hydrogen after the condensable component was frozen out, and the temperature where the condensation took place (at 16°K instead of the usual 20°K). All these samples for the analysis were taken from the same storage balloon, filled with a mixture of H<sub>2</sub>-CO. It was found that in spite of the variations the results of our analysis were reproducible within 2%.

When the condensable component in our analysis circuit was frozen out and removed, the remaining "pure hydrogen" was analysed a second time; it was found that there remained less than 0.00003% of impurities in this gas. Thus we concluded that the number of successive circulations (there were actually 6) during the freezing-out period proved to be satisfactory and that the whole amount of impurities was removed.

With respect to the consistency of the tests of the analysis procedure the experimental values listed in the tables were given in three digits in most cases, although the actual total accuracy of the order of 2 to 4% would diminish with decreasing temperature. The isobar at 1.3 atm is systematically less accurate as a result of difficulties involved in the sampling of the gas at this low pressure; the

whole arrangement was, indeed, designed for work at high pressures only.

§ 15. *Discussion of results.* The experimental data for  $H_2-N_2$  mixture are represented in fig. 20; the horizontal scale corresponds

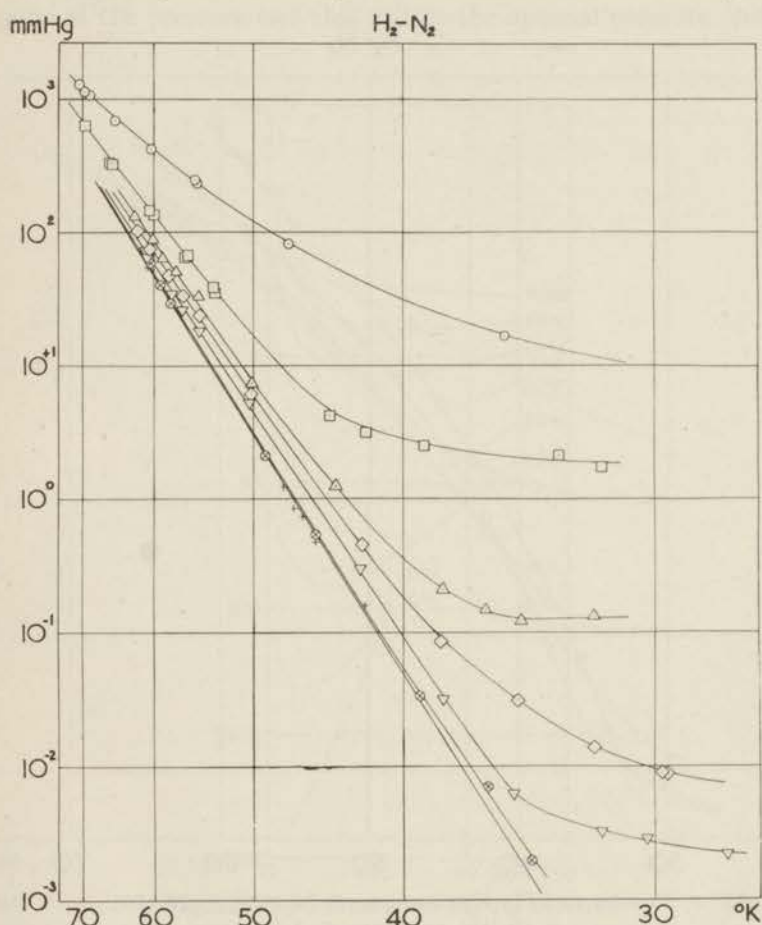


Fig. 20. Partial pressure of  $N_2$  in  $H_2$  as a function of temperature at constant pressures: ○ 50 atm, □ 25 atm, △ 15 atm, ◇ 10 atm, ▽ 5 atm, ⊗ 1.3 atm, + vapour pressure points of  $N_2$ .

to the reciprocal temperature; the logarithm of the partial pressure is plotted along the vertical axis. Thus the vapour pressure curve of pure nitrogen corresponds to a straight line. In this representation

the curves corresponding to the same total pressure do not intersect each other in contrast to fig. 21 where the concentration curves (logarithmically given as a function of the linear temperature) do intersect each other. Fig. 20 shows that the partial pressure of nitrogen increases with the increasing total pressure at a constant temper-

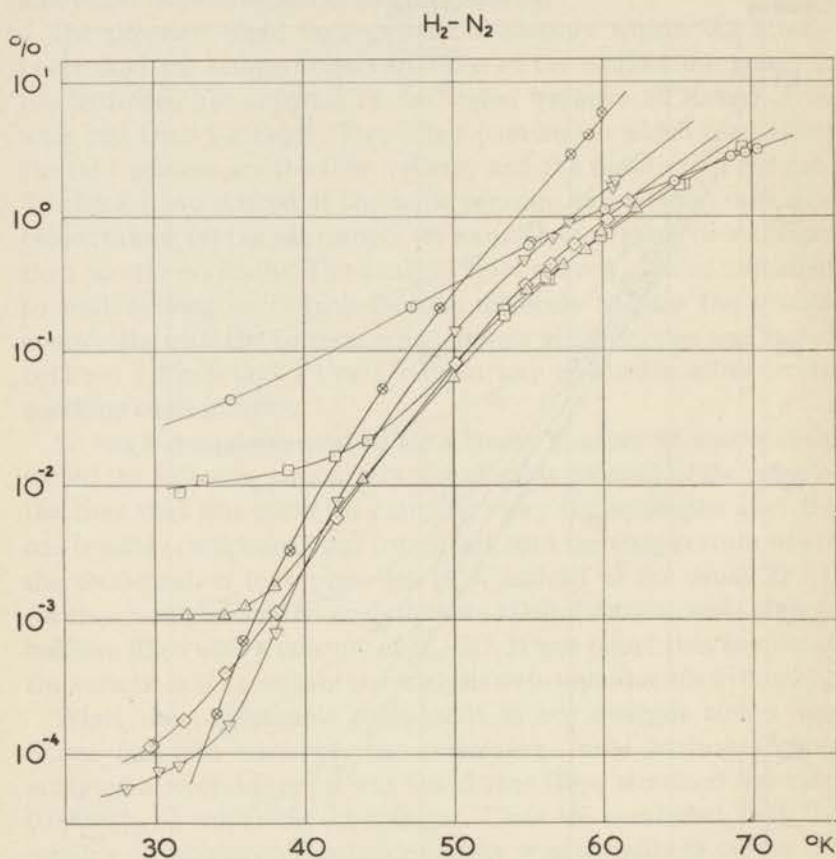


Fig. 21.  $x$ ,  $T$ -isobars of  $H_2$ - $N_2$ -mixture:  $\circ$  50 atm,  $\square$  25 atm,  $\triangle$  15 atm,  $\diamond$  10 atm,  $\nabla$  5 atm,  $\otimes$  1.3 atm.

ature; according to fig. 21, however, there is no such analogous relation between the concentrations and the pressure at a constant temperature.

The envelope of the system of  $T$ ,  $x$ -isobars gives with respect to the temperature axis the minimum attainable concentration of the

gas phase. Therefore, if we want to reach this minimum of concentration, a certain optimal pressure must be fixed. The determination of this optimal pressure may be achieved in the following way: from the isobars (see fig. 21) we can easily determine a set of  $p, x$ -isotherms (see fig. 22); the concentration minima correspond to a certain value of the pressure and this will be the optimal pressure plotted

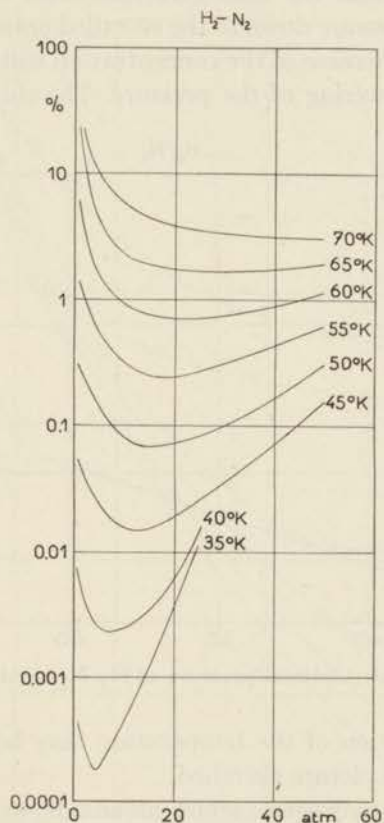


Fig. 22.  $x, p$ -isotherms of  $H_2-N_2$ -mixture.

in fig. 23 as a function of the temperature. This diagram shows a pronounced difference of the slope of both approximately linear parts at about the triple point temperature of nitrogen.

This characteristic behaviour of the mixture  $H_2-N_2$  is, of course, consistent with the qualitative picture of the  $p, T, x$ -space model (see section 3), so that we shall now better understand our results.

The  $T, x$ -isobars give the profile curves of the  $p, T, x$ -surface corresponding to the constant value of the third coordinate axis. For instance, it follows immediately that the isobars for higher pressures (50 or 25 atm respectively) will finally remain approximately constant at a relatively large distance from the hydrogen axis, even at temperatures below the critical temperature of hydrogen. Further it will be evident that the concentrations must decrease with the decreasing total pressure down to the so-called optimal pressure, and that a retrograde increase of the concentration will follow as a result of a subsequent lowering of the pressure. The shift of the optimal

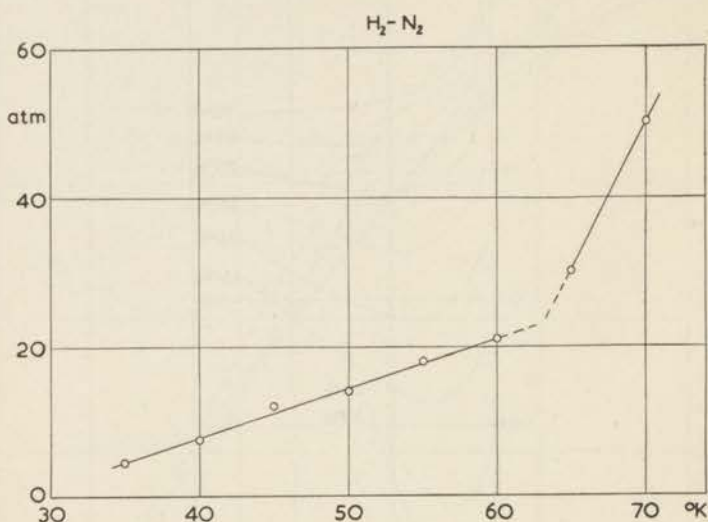


Fig. 23. Optimal pressure of  $H_2-N_2$ -mixture.

pressure as a function of the temperature may be seen as another consequence of the picture sketched.

For the system hydrogen-carbon monoxide we constructed the corresponding diagrams as in the case of the system hydrogen-nitrogen: the partial pressure of carbon monoxide in hydrogen is shown in fig. 24, the isobars in fig. 25, the isotherms in fig. 26 and the optimal pressure as a function of the temperature in fig. 27. A discussion similar to the one we gave for the system hydrogen-nitrogen would, of course, also apply to the system hydrogen-carbon-monoxide.

## CHAPTER V. COMPARISON OF THEORY AND EXPERIMENT

§ 16. *General  $p$ ,  $T$ -theory.* It would be possible to compare the theory with the experimental data by means of the corresponding pairs of figs. 13 and 21, or 12 and 20; the first pair, however, is not

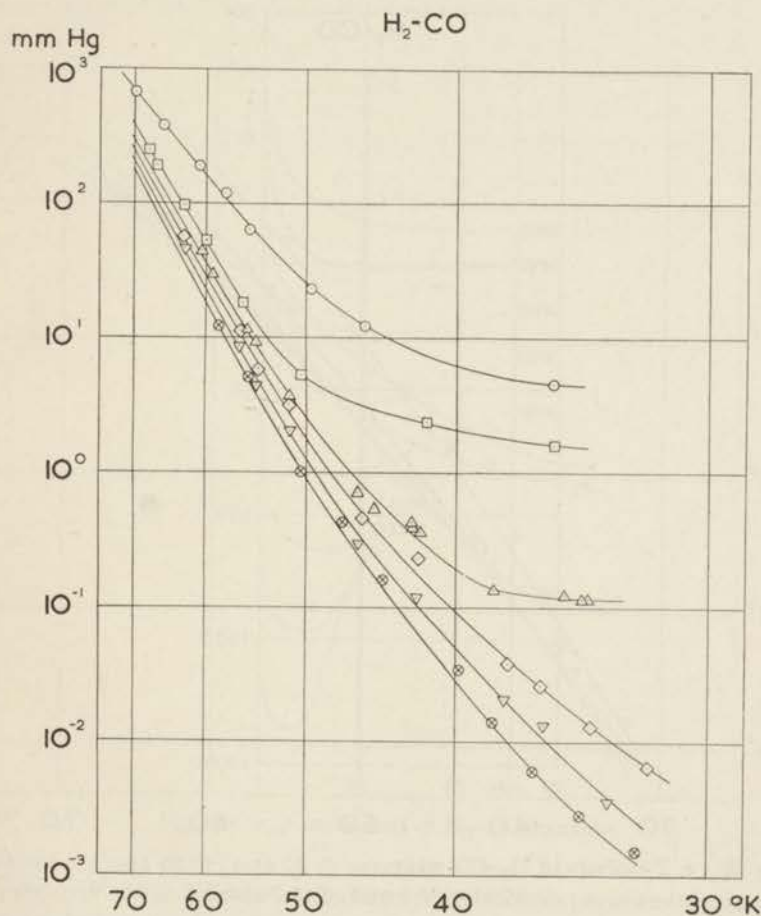


Fig. 24. Partial pressure of CO in H<sub>2</sub> as a function of temperature at constant pressure: ○ 50 atm, □ 25 atm, △ 15 atm, ◇ 10 atm, ▽ 5 atm, ⊗ 1.3 atm.

convenient because of a considerable density of theoretical and experimental curves in the vicinity of the envelope of the system of these curves.

The experimental points plotted in diagram 20 show a satisfactory agreement with the theoretical predictions (see fig. 12) at temperatures from 70°K down to about 44°K and at pressures up to 20 atm; the disagreement with the linear  $p, T$ -theory appears at temperatures below 44°K and at pressures higher than 20 atm.

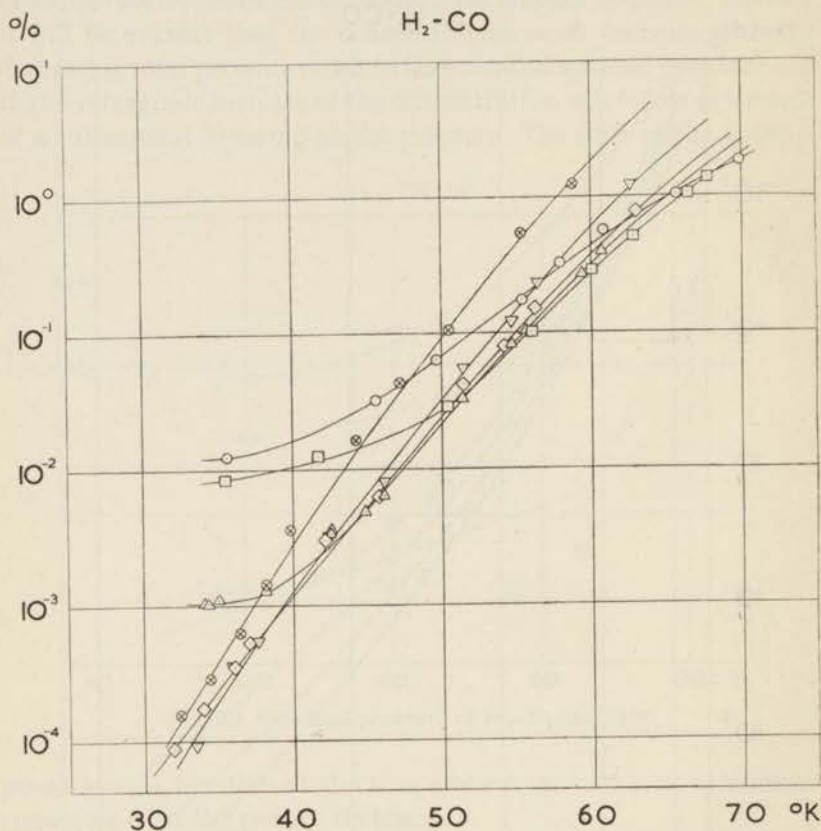


Fig. 25.  $x, T$ -isobars of H<sub>2</sub>-CO-mixture: ○ 50 atm, □ 25 atm, △ 15 atm, ◇ 10 atm, ▽ 5 atm, ⊗ 1.3 atm.

We prefer to compare the results from theory with the measured data, using the diagrams containing the enhancement factor as a function of the pressure at several fixed temperatures; therefore, we determined the experimental values of  $f$  for 50, 25, 15, 10 and 5 atm and plotted them in fig. 28 for the same series of temperatures as we have used for the numerical evaluation of the linear theory.

As shown in the diagram, the theoretical straight lines which correspond to the linear approximation are drawn only up to about 20 atm pressure. Evidently, we find again the same area of agreement as stated above.

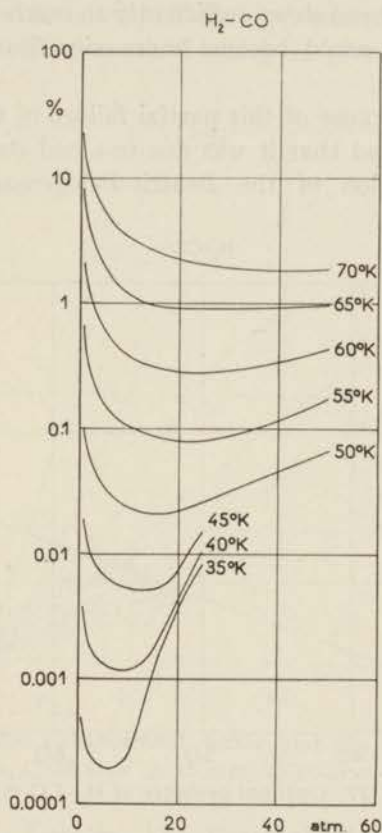


Fig. 26.  $x, p$ -isotherms of  $H_2$ -CO-mixture.

From fig. 28 it follows immediately that the experimental curves are parabolae of at least the third order. When physically interpreted according to (19) this means that it would be necessary to evaluate numerically at least the quadratic and the cubic terms of (19) in order to reach the desired agreement with the measurements for pressures higher than 20 atm and temperatures lower than 44°K.

Therefore, we took the typical isotherm of 40°K separately, reproduced this curve in fig. 29 with the corresponding linear

enhancement factor, and also computed the quadratic and the cubic term of (19) for this case. Indeed, we see that the quadratic curve is appreciably raised compared with the theoretical linear curve. At pressures of about 40 to 50 atm the cubic  $p, T$ -curve, however, does not bend down sufficiently to reach the experimental curve; this effect would become more significant for pressures higher than 70 atm.

We studied the cause of this partial failure of the general  $p, T$ -theory and we found that it was due to a bad convergence of the approximate solution of the Beattie-Bridgeman equation (15)

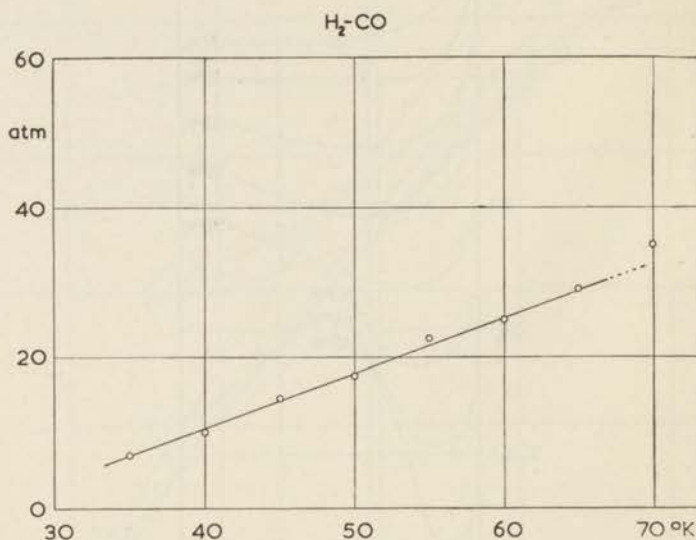


Fig. 27. Optimal pressure of H<sub>2</sub>-CO-mixture.

necessary for the integration of the corresponding expansion in powers of the pressure (see (19)). Indeed, we may not expect that the formula for  $f$  would give consistent results for any value of the pressure; we actually found that (15) already gives nonreproducible results for the compressibility data of pure hydrogen at pressures higher than 25 atm. Moreover, as the adjustment of the Beattie-Bridgeman constants represents another difficult problem at low temperatures, we do understand the natural limitation of the general  $p, T$ -theory.

As the result of a systematic examination we further found that

the analytically determined area of convergence of the  $p, T$ -theory indeed coincides with the region of agreement between the  $p, T$ -theory and the results of the measurements performed.

For the theoretical approach of our experimental results beyond the validity of the discussed  $p, T$ -theory it was necessary to develop another more powerful method which is given in the following section.

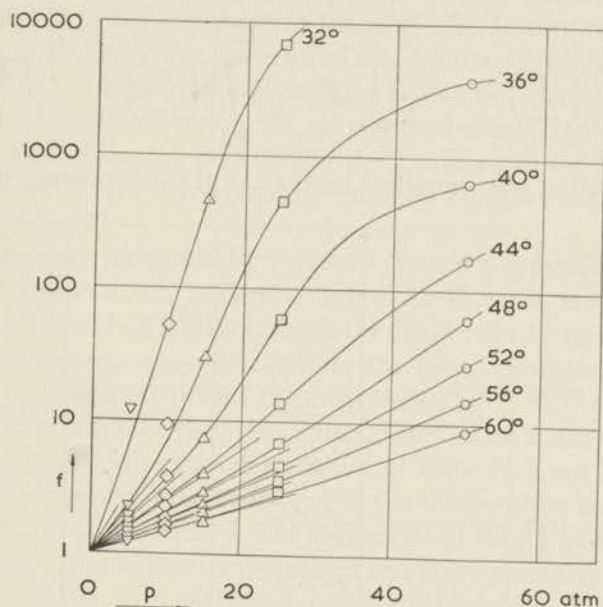


Fig. 28. Experimental enhancement factor and the linear  $p, T$ -theory.  
 ○ 50 atm, □ 25 atm, △ 15 atm, ◇ 10 atm, ▽ 5 atm.

§ 17. *General  $V, T$ -theory.* The Beattie-Bridgeman equation of state has been theoretically developed and experimentally tested in the original form (12); when we calculated the  $p, T$ -theory, however, we did not work with this equation (12) but with the corresponding approximate solution (13), which did not converge at certain higher pressures \*). We developed, therefore, the  $V, T$ -theory which proved to be powerful enough to reach an agreement with our experimental data. The computation of the same isotherm at 40°K (see fig. 29) again proved to be a crucial test of the theory.

\*) We are indebted to Dr. N. W. Roberts for valuable suggestions concerning the theoretical investigations.

The method of calculation explained for the  $p, T$ -theory in chapter II was followed in this case. The substitution of the corresponding chemical potentials in  $V, T$ -variables into the Gibbs equilibrium condition resulted in the following relation for the enhancement factor:

$$\ln f = \ln \frac{Vp}{V_{01}p_{01}} + \frac{1}{RT} \int_{p_{01}}^p v_{01} dp - \frac{1}{RT} \int_V^{\infty} \left[ \left( \frac{\partial p}{\partial n_1} \right)_{v,T,n} - \frac{RT}{V} \right] dV + \frac{1}{RT} \int_{V_{01}}^{\infty} \left[ \left( \frac{\partial p}{\partial n_1} \right)_{v,T} - \frac{RT}{V} \right] dV. \quad (29)$$

This equation was simplified by the use of the formalism developed

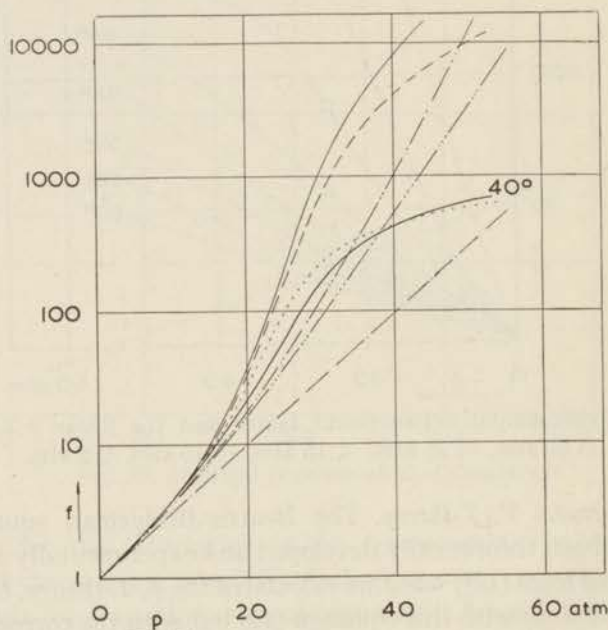


Fig. 29. Comparison of the  $f$ -curve at  $40^\circ\text{K}$  with the theory: the curve marked — is experimentally found; the curve marked -.- is computed from the linear  $p, T$ -theory; the curve marked -...- is computed from the quadratic  $p, T$ -theory; the curve marked -...-... is computed from the cubic  $p, T$ -theory; the curve marked — is computed from the linear  $V, T$ -theory; the curve marked - - - - is computed from the quadratic  $V, T$ -theory; the curve marked . . . . . is computed from the cubic  $V, T$ -theory.

in sections 6 and 7. The elimination of negligible terms finally gave the expansion in ascending powers of the reciprocal volume  $1/V$ :

$$\ln f = \ln \frac{Vp}{V_{01}p_{01}} + \frac{v_{01}p}{RT} - \frac{2\beta_{12}}{RT} \frac{1}{V} - \frac{2\gamma_{12} + \gamma_2}{2RT} \frac{1}{V^2} - \frac{2\delta_{12} + 2\delta_2}{3RT} \frac{1}{V^3}. \quad (30)$$

This equation enables us to classify again three degrees of approximation, namely the linear, the quadratic and the cubic  $V, T$ -theory with respect to the expansion in terms of  $1/V$ . In contrast with the general  $p, T$ -theory, the lower virial coefficients do not interfere any more with the higher approximations as was the case in (19).

We took the same values for all parameters as listed in (27) and (28) and we evaluated numerically the formula (30) for the temperature of  $40^\circ\text{K}$ ; the corresponding three  $V, T$ -curves are also represented in fig. 29.

We see that the linear  $V, T$ -theory gives the typical S-like form of the characteristic isotherms below  $42^\circ\text{K}$  while the quadratic  $V, T$ -curve is shifted a little towards the one obtained experimentally, but it seems necessary to compute the cubic correction to reach satisfactory agreement with the measurements.

As a conclusion of these theoretical discussions it may be stated that the Beattie-Bridgeman equation of state does not fit exactly the data for hydrogen and nitrogen in the temperature and pressure range we have investigated. The agreement of theory and of experiment is better at higher temperatures and lower pressures. The error becomes greater with decreasing temperatures and higher pressures and is sufficient to account completely for the discrepancy between the observed and calculated results.

## CHAPTER VI. THE TERNARY SYSTEM HYDROGEN-NITROGEN-CARBON MONOXIDE

§ 18. *Two-phase equilibrium of three component system.* The standard representation of a ternary system at a constant pressure and temperature is shown in fig. 30 for the special case of a two-phase equilibrium where the gas curve A-B is separated from the liquid curve K-L; for instance, this may be the case with a gas-liquid equilibrium of the ternary system hydrogen-nitrogen-carbon monoxide as it was investigated by Verschoyle<sup>2)</sup> or Ruhemann and Zinn<sup>6)</sup>. Remembering that the vertices of the triangle diagram



With the existing analysis apparatus for binary mixtures it would be possible to measure the corresponding concentration of the condensable components of the ternary gas mixture  $H_2-N_2-CO$  at liquid hydrogen temperature. For the determination of the relative concentration of  $CO$  with respect to  $N_2$ , we built according to Tompkins and Young<sup>23)</sup> an additional apparatus that is shown diagrammatically in fig. 31.

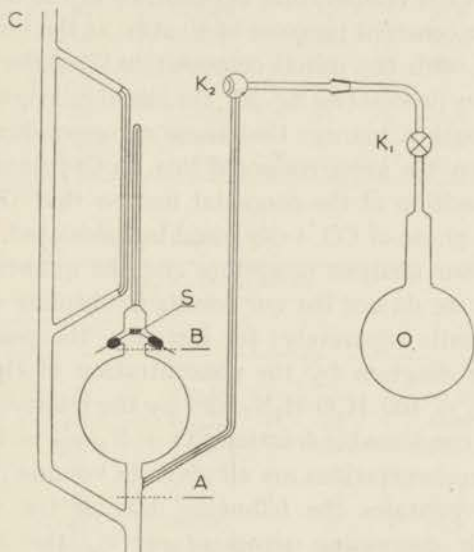


Fig. 31. Analysis of  $CO-N_2$ -gas mixture.

The apparatus, consisting of a MacLeod gauge, was provided with a platinum filament  $S$  and a capillary inlet for the introduction of oxygen from the balloon  $O$ . The complete gas analyser was connected with the circulating circuit at  $C$  parallel to the other MacLeod gauge  $Ml_1$  (see fig. 18). The stopcock  $K_2$  was closed and the total concentration of both condensable components together was first determined in the same way as in the case of the analysis of a binary gas mixture. At the end of this procedure the known quantity of  $N_2 + CO$  was thus already introduced into the bulb ( $= \frac{1}{2} l$ ) and the mercury level was adjusted at  $A$ . The space between  $K_1$  and  $K_2$  was filled with oxygen of an appropriate pressure from the storage balloon  $O$ , and by rotating the partially drilled stopcock  $K_2$  we could conveniently withdraw a small amount of oxygen into the bulb.

After the measurement of the pressure the mercury was lowered down to the level *B* in the small combustion space just above the bulb, and the filament was flashed at red heat. From the pressure decrease and the previously recorded data we calculated the relative composition of CO.

§ 20. *Experimental data of the mixture H<sub>2</sub> - N<sub>2</sub> - CO.* We investigated first the temperature dependence of the ternary mixture H<sub>2</sub>-N<sub>2</sub>-CO at a constant pressure of 10 atm; as the resulting composition *C* varies with the initial composition *C*<sub>0</sub> of the mixture when starting the flow process (see fig. 30), the initial mixture was repeatedly chosen in such a manner that these corresponding points lay in the diagram on the same connodal line. Both points *C*<sub>0</sub> and *C* determine the position of the connodal line so that the composition *C*<sub>s</sub> of the solid phase of CO + N<sub>2</sub> could be calculated.

As regards our analysis procedure and the quantitative concentration values we do not list our results in absolute concentrations of all components separately; for instance, the point *C*<sub>0</sub> may be located in the diagram by the concentration of the condensable components *c*'<sub>0</sub> = 100 H<sub>2</sub>D/H<sub>2</sub>N<sub>2</sub> and by the relative concentration of CO in the condensable fraction CO + N<sub>2</sub>, *c*'<sub>01</sub> = 100 DC'<sub>0</sub>/DE in %. Thus the concentrations are all given in volume percentages.

Table XIV contains the following data of the 10 atm isobar arranged with decreasing temperature: *c*<sub>0</sub>, the initial concentration of the condensable components; *c*<sub>01</sub>, the relative concen-

TABLE XIV

H <sub>2</sub> -N <sub>2</sub> -CO isobar at 10 atm						
<i>T</i> °K	<i>c</i> <sub>0</sub>	<i>c</i> <sub>01</sub>	<i>p</i> <i>x</i> <sub>12</sub>	<i>c</i>	<i>c</i> <sub>1</sub>	<i>c</i> <sub>s</sub>
66.0	4.22	50	162	2.22	43	57.2
60.8	4.22	50	63.2	0.824	32	55.9
58.4	4.22	50	36.5	0.480	29	52.5
56.6	1.80	48.3	25.3	0.333	26	53.0
55.6	4.22	50	18.4	0.242	27	51.2
52.8	1.80	48.3	9.06	0.119	23	50.2
50.1	1.80	48.3	3.74	0.0483	22	49.0
47.4	1.80	48.3	1.97	0.0260	21	48.5
45.3	1.80	48.3	1.178	0.0155	21	48.4
42.5	1.80	48.3	0.359	0.00472	23	48.3
39.3	1.80	48.3	0.107	0.00141	21	48.3
35.0	1.80	48.3	0.0228	0.000297	19	48.3

TABLE XV

H <sub>2</sub> -N <sub>2</sub> -CO at 50 °K						
$p$ atm	$c_0$	$c_{01}$	$c$	$c_1$	$c_s$	Remarks
5		0	0.140	0	0	E
5	1.99	30	0.081	10	30.8	
5	2.40	48.8	0.0616	27.4	48.8	
5		100	0.0325	100	100	E
10		0	0.0780	0	0	E
10	1.99	30	0.0559	12	30.5	
10	2.40	48.8	0.0500	22	48.8	
10		100	0.0240	100	100	E
15		0	0.0665	0	0	E
15	1.99	30	0.0565	11	30.8	
15	2.40	48.8	0.0440	24	48.8	
15		100	0.0215	100	100	E

TABLE XVI

H <sub>2</sub> -N <sub>2</sub> -CO at 45°K						
$p$ atm	$c_0$	$c_{01}$	$c$	$c_1$	$c_s$	Remarks
5		0	0.0235	0	0	E
5	1.12	30	0.0143	16	30.2	
5	2.40	48.8	0.0123	22	48.8	
5		100	0.00670	100	100	E
10		0	0.0150	0	0	E
10	1.12	30	0.0124	12	30.2	
10	2.40	48.8	0.0100	21	48.8	
10		100	0.00535	100	100	E
15		0	0.0155	0	0	E
15	1.12	30	0.0141	11	30.2	
15	2.40	48.8	0.0129	22	48.8	
15		100	0.00510	100	100	E

tration of CO in the condensable fraction in the initial mixture;  $p x_{12}$  the partial pressure of the condensable components in the gas phase in mm Hg;  $c$ , the concentration of the condensable components in the gas phase;  $c_1$ , the relative concentration of CO in the condensable fraction in the gas phase;  $c_s$ , the calculated relative concentration of CO in the solid state.

We plotted the concentration  $c$  against the temperature  $T$  in fig. 32; for a comparison we added the corresponding curves for a H<sub>2</sub>-N<sub>2</sub> mixture (the upper curve) and for a H<sub>2</sub>-CO mixture (the lower curve). The temperature dependence of the concentration of CO in the gas phase and in the solid phase is shown in fig. 33. In

both cases the CO relative concentration decreases with decreasing temperature. There is a remarkable shift of the relative CO-concentration with respect to the initial CO-concentration in the gas phase. The relative concentration of CO in the solid phase, however, approximates asymptotically the initial relative concentration of CO because the whole amount of CO + N<sub>2</sub> practically remains in the equilibrium vessel.

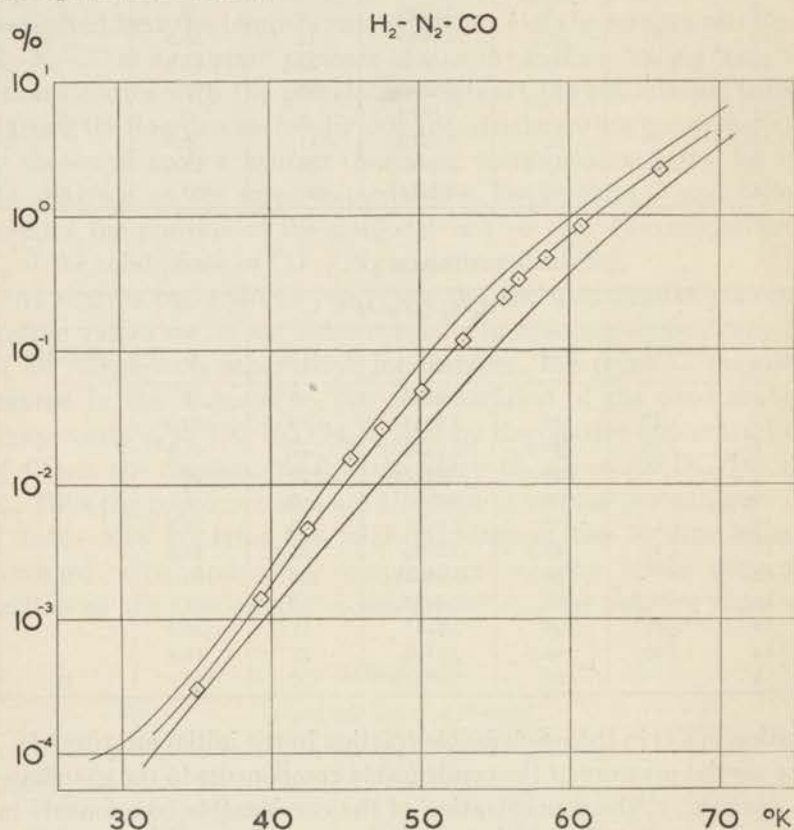


Fig. 32.  $x$ ,  $T$ -isobar of H<sub>2</sub>-N<sub>2</sub>-CO-mixture for  $c_{01} = 50\%$  at 10 atm. ( $\diamond$ ). The upper curve represents the  $x$ ,  $T$ -isobar of H<sub>2</sub>-N<sub>2</sub>-mixture at 10 atm; the lower curve represents the  $x$ ,  $T$ -isobar of H<sub>2</sub>-CO-mixture at 10 atm.

The diagrams in fig. 32 and 33 enable us, of course, to plot the gas curve ACB (see fig. 30) for any temperature at the pressure of 10 atm; two examples are given in fig. 34 for 50°K and 45°K.

The pressure dependence was investigated for two temperatures:

50°K and 45°K. The corresponding experimental data are reproduced in tables XV and XVI. We used the same respective symbols as in table XIV, E stands for an interpolated value from the corresponding binary equilibrium diagrams.

For the construction of the gas curves in fig. 34 it was satisfactory to draw only the enlarged tops of the complete triangle diagrams; the arrows are pointing towards both vertices of  $N_2$  and CO and towards the points representing the initial compositions  $C_0$  (see also fig. 30).

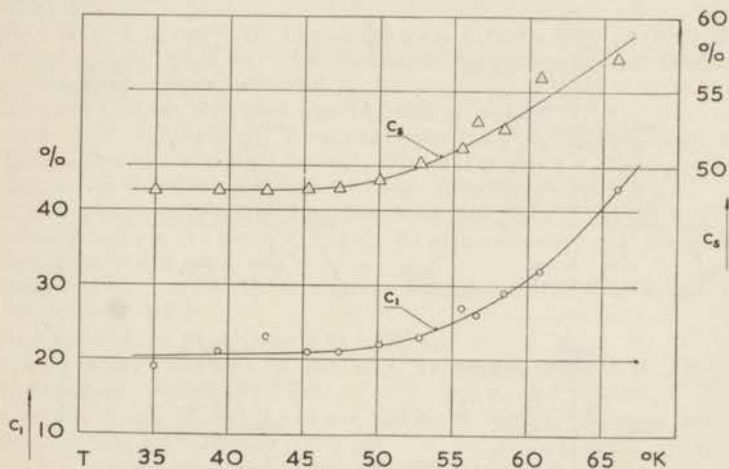


Fig. 33. The temperature dependence of  $c_1$  and  $c_s$ .

The remarkable shift of the upper ends of the connodal lines towards lower relative CO-concentrations proves to be a general characteristic feature of the hydrogen-nitrogen-carbon monoxide system as it was first found in the case of higher temperatures by Ruhemann and Zinn<sup>6)</sup> in contrast to the diagrams of Verschöyle<sup>2)</sup>.

The straight line connecting both binary points on the triangle sides can already represent the ternary gas curve in first approximation as was expected. From the inspection of the actual gas curves we conclude that there is a systematic pressure dependence of the curvature of the corresponding curves: the concave curves at 5 atm change into approximately straight lines at about 10 atm and at 15 atm the curves are slightly convex. Also this behaviour is consistent with measurements at higher temperatures<sup>2) 6)</sup>.

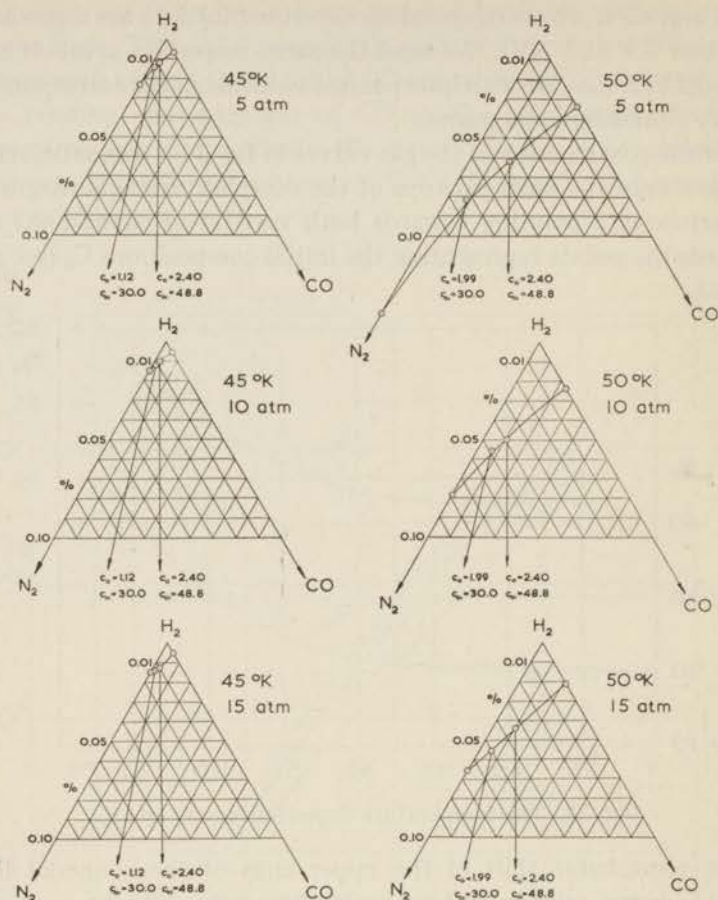


Fig. 34. Equilibrium curves of  $H_2-N_2-CO$ -system for 45°C and 50°C at 5, 10 and 15 atm.

This work was supported by a Research Grant from the British Atomic Energy Research Establishment, Harwell. We wish to express our sincere thanks to Mr. L. Neuteboom for his technical help.

## REFERENCES

- 1) Bakhuis Roozeboom, H. W., Die heterogenen Gleichgewichte, 2. Heft, Friedrich Vieweg und Sohn, Braunschweig, 1904.
- 2) Verschoyle, T. T. H., Trans. Roy. Soc. London (A) **230** (1931) 189.
- 3) Hoge, H. J. and G. J. King, NBS-NACA Table 11.50.
- 4) Wooley, W., B. Scott and F. G. Brickwedde, J. Res. Nat. Bur. Stand. **41** (1948) 379.
- 5) Ruhemann, M., The separation of gases, Oxford University Press 1949.
- 6) Ruhemann, M. and N. Zinn, Phys. Z. USSR. **12** (1937) 389.
- 7) Beattie, J. A., Chem. Rev. **44** (1949) 141.
- 8) Beattie, J. A. and O. C. Bridgeman, Proc. Amer. Acad. Arts Sci. **63** (1928) 229.
- 9) Beattie, J. A. and W. H. Stockmayer, J. Chem. Phys. **10** (1942) 473.
- 10) Waals, J. D. van der, Die Continuität des gasförmigen und flüssigen Zustandes, Barth, Leipzig, 1899-1900.
- 11) Lorentz, H. A., Ann. Phys. Lpz. **12** (1881) 127 and 660.
- 12) Urk, A. T. van and H. Kamerlingh Onnes, Commun. Kam. Onnes Lab., Leiden No. 169e; Rep. Commun. first int. Comm. I.I.R., fourth int. Congr. Refr. No. 5b VI, 1924; Proc. fourth int. Congr. Refr. **1** (1924) 79a.
- 13) White, D., Bull. Eng. Exp. Stat. Ohio State Univ., June (1952) 12.
- 14) Kamerlingh Onnes, H. and C. Braak, Commun. No. 97a; Proc. K. Ned. Akad. Wet. **9** (1906) 754.
- 15) Nijhoff, G. P. and W. H. Keesom, Commun. No. 188e; Proc. K. Ned. Akad. Wet. **31** (1928) 413.
- 16) Schäfer, K., Z. Phys. Chem. B **36** (1937) 85.
- 17) Kamerlingh Onnes, H. and W. J. de Haas, Commun. No. 127c; Proc. K. Ned. Akad. Wet. **15** (1912) 405.
- 18) Smedt, J. de, W. H. Keesom and H. H. Mooy, Commun. No. 202a; Proc. K. Ned. Akad. Wet. **32** (1929) 745.
- 19) Dewar, J., Proc. Roy. Soc. London **73** (1904) 253.
- 20) Ruhemann, M., Z. Phys. **76** (1932) 380.
- 21) Vegard, L., Z. Phys. **88** (1934) 240.
- 22) Simon, F., M. Ruhemann and W. A. M. Edwards, Z. Phys. Chem. B **6** (1929) 331.
- 23) Tompkins, F. C. and D. M. Young, J. Sci. Instrum. **27** (1950) 224.

## SAMENVATTING

Dit proefschrift heeft tot onderwerp het evenwicht tussen de vaste fase en de gasfase van de systemen waterstof-stikstof, waterstof-koolmonoxyde en waterstof-stikstof-koolmonoxyde in het temperatuurgebied van 33°K tot 63°K en het drukgebied van 1,3 atm tot 50 atm.

In hoofdstuk I wordt een overzicht gegeven van de eigenschappen van de binaire systemen stikstof-koolmonoxyde en waterstof-stikstof. Het kwalitatieve gedrag van deze systemen voor een uitgebreid temperatuur- en drukinterval wordt beschreven met behulp van  $p,T$ -,  $T,x$ - en  $p,x$ -diagrammen, die worden afgeleid uit een driedimensionale representatie. Een bepaald deel van dit oppervlak correspondeert dus met het bovengenoemde programma van de metingen.

De te verwachten experimentele resultaten kunnen in benadering worden weergegeven met behulp van theoretische onderzoeken gebaseerd op de evenwichtsrelatie van Gibbs. In hoofdstuk II is de algemene theorie hiervan beschreven, en de met behulp van de toestandsvergelijking van Beattie-Bridgeman verkregen numerieke resultaten van de lineaire  $p,T$  theorie zijn graphisch weergegeven voor het binaire systeem waterstof-stikstof.

De experimentele methode, die voor het onderzoek van het fasen-evenwicht is toegepast, gebruikt een continu stromingsproces door een evenwichtsvat. De gebruikte opstelling wordt in hoofdstuk III beschreven; voor de analyse van de kleine hoeveelheden van  $N_2$  of CO, die zich met waterstofgas mengen, werd een methode ontwikkeld gebaseerd op het uitvriezen van  $N_2$  of CO bij de temperatuur van vloeibare waterstof.

Uit de resultaten van de binaire systemen, weergegeven in hoofdstuk IV, volgt dat er bij iedere temperatuur een optimale druk bestaat voor het bereiken van een minimale concentratie van stikstof of koolmonoxyde in de gasfase. In hoofdstuk V worden de

resultaten van het systeem  $H_2-N_2$  vergeleken met de theoretische beschouwingen uit hoofdstuk II. Het blijkt, dat de lineaire  $p,T$  theorie alleen bruikbare gegevens levert voor drukken tot 20 atm en voor temperaturen boven  $44^\circ K$ . Voor de  $40^\circ K$  isotherm worden ook de hogere benaderingen besproken. Kwantitatief blijkt echter de  $V,T$  theorie de genoemde isotherm in geheel het beschouwde meetbereik beter te beschrijven.

Tenslotte werden metingen verricht aan het ternaire systeem waterstof-stikstof-koolmonoxyde. De meetmethode en de daarbij noodzakelijke wijzigingen in het analyseapparaat worden in hoofdstuk VI beschreven. De samenstelling van het ternaire gasmengsel kan in goede benadering door lineaire interpolatie worden afgeleid uit de resultaten van de beide onderzochte binaire systemen  $H_2-N_2$  en  $H_2-CO$ .

Teneinde te voldoen aan het verlangen van de Faculteit der Wis- en Natuurkunde volgt hieronder een kort overzicht van mijn academische studie.

Na mijn aankomst in Nederland in 1948 werd ik door het Universitaire Asyl Fonds in staat gesteld mijn academische studie in Leiden voort te zetten, waar ik in April 1949 het kandidaats examen in de Wis en Natuurkunde aflegde. Vanaf dat tijdstip werkte ik op het Kamerlingh Onnes laboratorium, terwijl ik mij voorbereidde op het doctoraal examen in de experimentele natuurkunde, dat ik in October 1951 heb afgelegd. Hiervoor volgde ik de colleges van wijlen Prof. Dr H. A. Kramers, Prof. Dr J. Droste en Dr J. Korringa (thans te Columbus, Ohio).

In het laboratorium was ik tot 1951 werkzaam bij de werkgroep, die onder leiding van Prof. Dr K. W. Taconis stond. Daarna kreeg ik opdracht bepaalde eigenschappen van waterstofsysteem te gaan onderzoeken. De resultaten van dit werk vormen de inhoud van dit proefschrift.

Tenslotte zij nog vermeld, dat ik bij dit onderzoek bijgestaan werd door G. van Soest (1951-1952) en M. D. P. Swenker (1953).

## STELLINGEN

### I

De door Jeans gegeven toelichting op de definitie van het kritische punt kan aanleiding geven tot verwarring.

Sir J. Jeans, *An introduction to the kinetic theory of gases*, Cambridge University Press, 1946, p. 92.

### II

Volgens de theorie zou het mogelijk zijn met behulp van het systeem waterstof-stikstof temperaturen te bereiken, die nog lager liggen dan de temperaturen in een bad met vloeibare waterstof alleen; dit effect kan echter in de praktijk geen rol spelen.

H. W. Bakhuis Roozeboom, *Die heterogenen Gleichgewichte*, 2. Heft, Friedrich Vieweg und Sohn, Braunschweig, 1904, p. 213.

### III

Het Collins-toestel voor de liquefactie van helium, zoals dit in de standaard uitvoering door de fabriek wordt afgeleverd, kan vereenvoudigd worden, wanneer het helium gas in een gesloten systeem wordt rondgevoerd.

A. F. van Itterbeek, L. de Greve and H. Myncke, *Appl. Sci. Res. A* 3 (1952) 429.

### IV

Indien helium gas, verontreinigd met lucht, wordt gezuiverd door deze lucht uit te vriezen bij lage temperaturen, dient ter verkrijging van een zo groot mogelijke zuiverheid voor iedere temperatuur een bepaalde werkdruk te worden gekozen.

### V

Atkins et al. geven een methode voor het concentreren van  $^3\text{He}$  in het mengsel  $^3\text{He}$ - $^4\text{He}$ ; men kan de opbrengst van deze methode door een kleine wijziging van het toestel aanzienlijk verhogen.

K. R. Atkins, J. C. Findlay, D. R. Lovejoy and W. H. Watson, *Can. J. of Phys.* 31 (1953) 679.



## VI

De door Rydon and Smith beschreven methode voor het kleuren van peptiden en dergelijke verbindingen is niet specifiek voor de door hen aangegeven atoomgroepering.

H. N. Rydon and P. W. Smith, *Nature* **169** (1952) 922.

E. L. T. M. Spitzer, persoonlijke mededeling.

## VII

Op grond van de recente resultaten van Eelson over de dampspanningen van mengsels van  $^3\text{He}$ - $^4\text{He}$  kan worden ingezien, dat de theorie van de reguliere oplossingen niet kan worden toegepast op deze resultaten.

B. N. Eelson, *J. eks. i teor. fiz.* **26** (1954) 749.

H. S. Sommers jr., *Phys. Rev.* **88** (1952) 113.

## VIII

In de theorie van mengsels dient men het gebruik van het begrip „fugaciteit” zoveel mogelijk te vermijden.

## IX

In de theorie van relaxatieverschijnselen wordt doorgaans van de Fourier-transformatie gebruik gemaakt. De mathematische rechtvaardiging hiervan kan gebaseerd worden op het feit, dat bij deze verschijnselen noodzakelijkerwijze energie wordt gedissipeerd.

## X

De theorie gegeven in hoofdstuk II van dit proefschrift kan toegepast worden ter indirecte bepaling van de dampspanning van vaste stoffen.

## XI

Het is van groot belang de beschikbare radiogolven volgens een nieuw beginsel te verdelen daarbij rekening houdend met de eigenschappen van de moderne zendstations en ontvangtoestellen.

## VI

De door Lyden and Smith beschreven methode voor het leeren van partijen en hergeleide verbanden is niet specifiek voor de door hen aangegeven stouproestering.

E.L.M. HAYES and W. TALLEY, *Journal of Experimental Psychology*, 1952, 45, 217.

E.L.T. M. SARTER, *Personality and Individual Differences*, 1962, 1, 105.

## VII

De grond van de recente resultaten van Lyden over de draagvlakken van menselijke van 115-116 van worden logische, dat de theorie van de verhoogde oplossingen niet kan worden toegepast op deze resultaten.

E. H. HAYES, *Journal of Experimental Psychology*, 1952, 45, 217.

E. H. HAYES, *Journal of Experimental Psychology*, 1952, 45, 217.

## VIII

In de theorie van menselijke draagvlak wordt gebruik van het gebruik van het gebruik van menselijke draagvlak te verbeteren.

## IX

In de theorie van relaxatieverschijnselen wordt doorgegaan van de theorie van relaxatieverschijnselen gebruik gemaakt. De mathematische verhouding tussen het gebruik van menselijke draagvlak op het feit, dat de verschillen in draagvlak tevens de draagvlak tevens.

## X

De theorie gegeven in hoofdstuk II van dit proefschrift kan toegepast worden ter indicatie van de draagvlak van de draagvlak van de draagvlak.

## XI

Het is van groot belang de beschreven methoden volgen van menselijke draagvlak te verbeteren draagvlak met de draagvlak van de draagvlak en draagvlak.

